4. Natural Time Analysis of Seismic Electric Signals

Abstract. The natural time analysis of all the measured SES activities showed that they are characterized by very strong memory and their normalized power spectra $\Pi(\omega)$ versus ω fall on a *universal* curve having $\kappa_1 (= \langle \chi^2 \rangle - \langle \chi \rangle^2)$ value equal to 0.070. This curve coincides with the one obtained on theoretical grounds when assuming that SES are governed by *critical* dynamics. Upon shuffling the events (pulses) randomly, the memory is destroyed and the κ_1 value becomes equal to that $\kappa_u (= 1/12 \approx 0.083)$ of a "uniform" distribution. This shows that the self-similarity *solely* stems from long range temporal correlations. Concerning the distinction of SES activities from similar looking "artificial" (man-made) noises, we find the following. Modern techniques of Statistical Physics, e.g., detrended fluctuation analysis (DFA), multifractal DFA, wavelet transform, when applied to the original time series *cannot* achieve such a distinction, but when they are applied in natural time a *clear* distinction emerges. For example, for the SES activities the DFA exponent in natural time is close to unity, i.e., $\alpha \approx 1$, while for "artificial" noises it is markedly smaller, i.e., $\alpha < 0.85$. Also the entropy S in natural time can achieve such a distinction: For SES activities *both* S and S_- (where S_- stands for the entropy in natural time under time reversal) are smaller than the entropy $S_u \approx 0.0966$ of the "uniform" distribution, which is *not* the case for the "artificial" noises where S is larger than (or equal to) S_u and S_- may either be smaller or larger than S_u. Upon "shuffling" the events (pulses) randomly, both values of S and S_- in the SES activities turn out to be equal to S_u, which conforms with the aforementioned conclusion that in SES activities the self-similarity originates solely from long range temporal correlations. Finally, when investigating the dependence of the fluctuations $\Delta\chi_l$ of the average value of natural time under time reversal versus the window length l, we can also achieve a distinction between SES activities and "artificial" noises. In particular, when studying the log-log plot of $\Delta\chi_l$ versus l, the former give *ascending* curves, in contrast to the latter that result in *descending* curves.

P.A. Varotsos et al., *Natural Time Analysis: The New View of Time: Precursory Seismic Electric Signals, Earthquakes and other Complex Time Series*, Springer Praxis Books, DOI 10.1007/978-3-642-16449-1_4,

4.1 Dichotomous time series. Markovian and non-Markovian processes

4.1.1 Difference between natural time analysis and earlier studies of dichotomous time series. The Markovian process

The following point should be stressed concerning one of the key differences of the natural time analysis compared to the earlier procedures in the study of *dichotomous* time series. For such time series, the quantity Q_k (see § 2.1.2, Fig. 2.1(a)) coincides with the so-called dwell time (for the high-level state *only*) and is one of the basic characteristics of a dichotomous (i.e., on–off) process. The standard procedure consists of the determination of the dwell times distribution $P(Q)$: for a Markovian process $P(Q)$ is *exponential*, i.e., $P(Q) = \mathrm{e}^{-Q/\overline{Q}}/\overline{Q}$ (frequently the average dwell time $\overline{Q}$ is different for the high- and the low-level states). For non-Markovian (which contain some "memory") processes $P(Q)$ is non-exponential, e.g., stretched exponential, i.e., of the form $\mathrm{e}^{-(Q/\tau)^b}$ where $0 < b < 1$, or even algebraic. On the other hand, the natural time analysis is carried out in terms of the *couple* (χ_k, Q_k), which takes into account the ordering of the pulses, and hence not *solely* based on the statistics of their durations, i.e., $P(Q)$.

We just mention here that ionic current fluctuations in membrane channels (ICFMC), the long-range correlations of which have been studied in Ref. [21], can be also approximated by dichotomous time series. Further, we clarify that (see Ref. [9] and references therein) single ionic channels in a membrane open and close spontaneously in a stochastic way, resulting in current and voltage changes which resemble the realizations of random telegraph signals (RTS, dichotomous noise). The channel's opening state can be determined [21] on the basis of the ion current: a low current corresponds to a closed channel state, while high current values indicate an open state (see Fig. 4.1). It has been shown [8] that the action of membrane-embedded enzymes depends critically on fluctuations of the membrane potential, and that the main source of these fluctuations originates in the fluctuations of ionic concentrations due to the action of ion channels. Recall that the SES activities have also an RTS feature, e.g., see Figs. 2.8 and 4.2. These figures also depict a number of "artificial" noises (see § 1.2.3) that have been intentionally selected to exhibit a RTS feature similar to that of SES activities. Note that N1–N5 and N9 of Fig. 4.2 correspond to n1–n5 and n6 of Fig. 2.8, respectively.

Hence, apart from a difference in the time-scales, the feature of *all* these electric signals is *similar* to that of the SES activities (RTS shape). This similarity instigated the simultaneous study of SES activities, "artificial" noises and ICFMC by Varotsos et al. [32, 34, 33], as will be explained below.

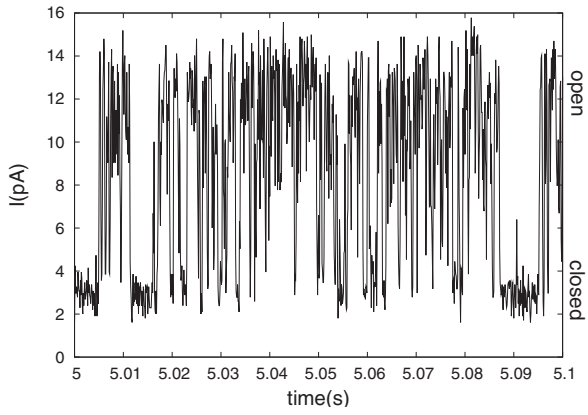

Fig. 4.1 Excerpt of the ionic current fluctuation in membrane channels (ICFMC) (f_{exp} =10 kHz) studied in Ref. [21] (see also Refs. [10, 9]).

4.1.2 Non-Markovian character of SES activities and "artificial" noises

Varotsos et al. [32] showed, by means of the Smoluchowski–Chapman–Kolmogorov functional equation (SCK equation), that the SES activities exhibit non-Markovian character (i.e., contain some "memory", see § 4.1.1). The stationarity of the signal was studied by the quantiles procedure. Subsequently, Varotsos et al. [33], in order to further investigate the non-Markovianity for both SES activities and "artificial" noises, proceeded to the study of the non-Markovian quantitative global measure G. Furthermore, they studied the coefficients of *skewness* and *kurtosis*.

The non-Markovian quantitative global measure G. Following Siwy and Fuliński [23], the definition of G can be summarized as follows: one of the properties of a Markov process is that it satisfies the SCK equation (e.g., see Ref. [32]). The deviation from this equation, i.e.,

$$D_{m,n}(t,\tau) = P(m,t|n,0) - \sum_{k=1}^{M} P(m,t|k,t-\tau)P(k,t-\tau|n,0), \tag{4.1}$$

measures the degree of non-Markovianity. In Eq. (4.1), the indices $k,m,n = 1,2,\ldots M$ number the electric field states (note that in our case we have $M = 2$ different states, labeled "high", $m = 1$, and "low", $m = 2$, respectively; we consider as *"high"-level states* those having the *largest* deflections of the electric field amplitude with respect to the background level; see the arrows in Fig. 4.2). The $P(m,t|n,s)$ stands for the field–field conditional probability that the electric field $E(t)$ is in the state number m, under the condition that at the earlier time $s < t$ the field $E(s)$ was in the state number n.

The integral measure (mean square characteristics) of the non-Markovianity is [9, 23]

$$G = G(\tau,T) = \left[\frac{1}{T}\frac{1}{M^2}\sum_{m,n}^{M}\int_{\tau}^{\tau+T} D_{m,n}^2(t,\tau)\,\mathrm{d}t\right]^{1/2} \tag{4.2}$$

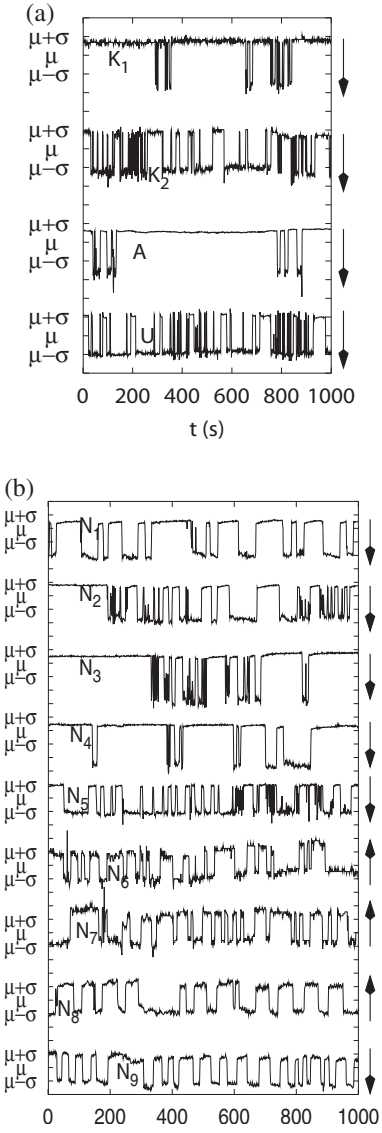

Fig. 4.2 Excerpts of: (a) four SES activities recorded on April 18, 1995 (K1), April 19, 1995 (K2), March 17, 2001 (A) and February 5, 2002 (U); (b) nine "artificial" noises recorded on November 14, 1997 (N1), November 15, 1997 (N2), November 16, 1997 (N3, N4 and N5), July 13, 2001 (N6), August 4, 2001 (N7), March 22, 2001 (N8 and N9). The SES activity U was recorded at IOA (see Ref. [34]), while for the SES activities K1, K2 and A see the caption of Fig. 4.5. The "artificial" noises were distinguished from SES activities according to the criteria discussed in Section 1.2, and collected at various stations (see the map of Fig. 1.2), i.e., N1 to N5 at VOL, N6 and N7 at IOA, N8 and N9 at LAG (this is a station lying very close to ASS). The electric field E is presented here in *normalized* units (μ and σ stand for the mean value and the standard deviation in each case, respectively). The arrows on the right indicate the polarity of the deflection from the background level to the largest (in amplitude) electric field variations (i.e., from the "low"-level to the "high"-level states). Taken from Ref. [34]. Note that N1–N5 and N9 correspond to n1–n5 and n6 of Fig. 2.8, respectively.

where T is the range of the time t and τ is the shift in the SCK equation. As an example, for the SES activity K1 and the "artificial" noise N1 mentioned in Fig. 4.2, the calculation for $T = 100$ s yields $G_{max}(= \sup_\tau G(\tau, T)) = 0.107 \pm 0.002$ and 0.135 ± 0.004, respectively. For computer-generated Markovian dichotomous series of comparable length, the corresponding G values are smaller by one order of magnitude, which also suggests the non-Markovian character of the experimental data for both cases, i.e., K1 and N1, respectively (this non-Markovianity has been also shown by employing the entropy fluctuations

δS in natural time and the relevant complexity measures; see Table 4.5 and the last paragraph of § 9.1.2).

Skewness and kurtosis. The coefficients of skewness (γ_1) and kurtosis (β_2) are (see p. 928 of Ref. [1]):

$$\gamma_1 = \mu_3/\sigma^3 \text{ and } \beta_2 = \mu_4/\sigma^4 \tag{4.3}$$

where μ_n denotes the nth central moment, i.e., $\mu_n = \sum_s (x_s - \mu)^n p_s$ for randomly distributed data x_s with point probabilities p_s. The symbol μ stands for the mean and σ for the standard deviation. For Markovian processes, the durations of the "high"- (T_h) and "low"-level states (T_l) should follow exponential distributions $p(\mathrm{T}) = \lambda \exp(-\lambda \mathrm{T})$ (see § 4.1.1), for which the values $\gamma_1 = 2$, $\beta_2 = 9$ and $\sigma^2/\mu^2 = 1$ are expected. The two coefficients γ_1 and β_2 are tabulated along with σ^2/μ^2 in table II of Ref. [28], for both series of the "high"- and "low"-level states' durations of the "artificial" noises and the SES activities depicted in Fig. 2.8. Comparing these values with those expected from an exponential distribution, we find [33] the following: None of the time series of durations, corresponding to either the SES activities or the "artificial" noises investigated, could be compatible with an exponential distribution. Moreover, the Kolmogorov-Smirnov test excludes for the SES activities the Gaussian distribution.

In short, both the SES activities and the "artificial" noises exhibit non-Markovian character.

4.1.3 Markovian dichotomous time series. Spectral analysis and detrended fluctuation analysis (DFA)

This was studied in Ref. [33]. Following Berezhkovskii and Weiss [6], in the case of a Markovian dichotomous (M =2, m =1,2; these are the symbols used in § 4.1.2) time series, the probability densities for the time spent in a single sojourn in the states "high" ($m = 1$) and "low" ($m = 2$) respectively are *both* exponential, i.e.,

$$p_1(T) \propto \exp(-T/\tau_{high}), \;\; p_2(T) \propto \exp(-T/\tau_{low}) \tag{4.4}$$

and lead to the following expressions for the field–field conditional probabilities

$$P(1,t+\tau|1,t) = \tau_{eff}\left[\frac{1}{\tau_{low}} + \frac{\exp(-\tau/\tau_{eff})}{\tau_{high}}\right] \tag{4.5}$$

and

$$P(2,t+\tau|1,t) = \frac{\tau_{eff}}{\tau_{high}}\left[1-\exp(-\tau/\tau_{eff})\right], \tag{4.6}$$

where $1/\tau_{eff} \equiv 1/\tau_{high} + 1/\tau_{low}$ and τ is a time lag. Note that the expressions of Eqs. (4.5) and (4.6) for the conditional probabilities satisfy the SCK functional equation (see § 4.1.2). The probability to observe the "high" state P_1 is

$$P_1 = \frac{\tau_{high}}{\tau_{low} + \tau_{high}}, \tag{4.7}$$

and the joint probability $P_{11}(\tau)$ to observe the "high" state at both the times t and $t+\tau$, due to the definition of the conditional probability, is

$$P_{11}(\tau) = P_1 P(1,t+\tau|1,t). \tag{4.8}$$

The power spectral density $S(\omega)$ is the Fourier transform of the autocovariance $\mathscr{C}(\tau) = \overline{[x(t+\tau)-\bar{x}][x(t)-\bar{x}]}$ of the stationary signal $x(t)$ [25] with average value $\bar{x}$:

$$\mathscr{C}(\tau) = \overline{x(t+\tau)x(t)} - \bar{x}^2 = \frac{1}{2\pi}\int_0^\infty S(\omega)\,\cos(\omega\tau)\,\mathrm{d}\omega. \tag{4.9}$$

If we assume that the states "low" and "high" have amplitudes 0 and ΔE, respectively, we have $\bar{x} = (\Delta E)P_1$, and $\overline{x(t+\tau)x(t)} = (\Delta E)^2 P_{11}(\tau)$, and using the expressions of Eqs. (4.5) and (4.7)–(4.9), we finally obtain

$$\mathscr{C}(\tau) = (\Delta E)^2 \frac{\tau_{eff}}{\tau_{low}+\tau_{high}} \exp\left(-\frac{\tau}{\tau_{eff}}\right) \tag{4.10}$$

Equation (4.10), using the Wiener–Khinchin theorem, leads to the power spectral density $S(\omega)$

$$S(\omega) = 4\int_0^\infty \mathscr{C}(\tau)\,\cos(\omega\tau)\,\mathrm{d}\tau = \frac{4(\Delta E)^2\tau_{eff}^2}{(\tau_{low}+\tau_{high})(1+\omega^2\tau_{eff}^2)} \tag{4.11}$$

The last relation reveals that the high-frequency behavior of the spectrum becomes $S(\omega) \propto \omega^{-2}$ if $\omega \gg (1/\tau_{high} + 1/\tau_{low})$, which corresponds to *a random walk-like behavior in short time-scales*. We will come back to this point below.

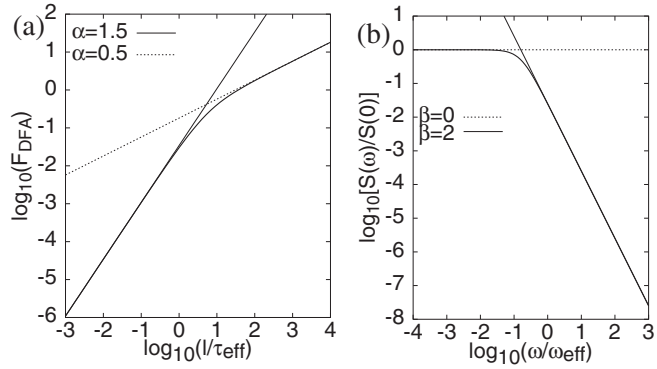

Fig. 4.3 Theoretical estimation of (a) the variability measure F_{DFA}(thick line) versus l/τ_{eff} and (b) the power spectral density $S(\omega)$ (thick line) versus ω/ω_{eff}, for a Markovian dichotomous signal (see § 4.1.3). The thin solid and dotted straight lines correspond to the short and long time ranges in each case, i.e., they are approached for $l \ll \tau_{eff}$ and $l \gg \tau_{eff}$, respectively. Taken from Ref. [33].

Following Talkner and Weber [25], the squared variability of DFA (§ 1.4.2) is given, in terms of $S(\omega)$, by:

$$F^2_{DFA}(l) = \frac{l}{2\pi}\int_0^\infty S(w/l) r_{DFA}(w)\, \mathrm{d}w \tag{4.12}$$

where w denotes the *dimensionless* frequency and $r_{DFA}(w)$ is given by the explicit form:

$$r_{DFA}(w) = [w^4 - 8w^2 - 24 - 4w^2\ \cos(w) + 24\ \cos(w) + 24w\ \sin(w)]/w^6. \tag{4.13}$$

In Fig. 4.3(a), the $F_{DFA}(l)$ versus l/τ_{eff} for a dichotomous Markovian process was drawn using Eqs. (4.11)–(4.13), while Fig. 4.3(b) depicts $S(\omega)$ versus ω/ω_{eff} where $\omega_{eff} \equiv 2\pi/\tau_{eff}$, using Eq. (4.11). This figure shows that [33]:

- Concerning the DFA exponent α: (i) For short time-scales (high frequencies), i.e., $\Delta t \ll \tau_{eff}$, the DFA exponent approaches the value $\alpha = 1.5$. (Note that such a behavior is expected for *any* signal with a *high* frequency spectrum as given in Eq. (4.11); see also below.) (ii) For long time-scales (low frequencies), i.e., $\Delta t \gg \tau_{eff}$, we find $\alpha = 0.5$, as expected. (iii) For intermediate scales, comparable to (or shorter than) τ_{eff}, DFA exponents exceeding unity (e.g., 1.2 or so) naturally emerge.
- Concerning the power spectrum exponent β (see § 1.4.2): it approaches the values 2 and 0 for the aforementioned short and long time-scales, respectively. For time-scales comparable to (or shorter than) τ_{eff}, values of β around unity or larger (e.g. $\beta = 1.4$) can fit the data. (In other words, data consisting, for example, of randomly distributed square pulses, if analyzed in the range $\Delta t \ll \tau_{eff}$, may approximately obey $S \propto \omega^{-\beta}$, $\beta \approx 1$.) Note that, for a given (high) frequency range, upon increasing $1/\tau_{eff}$ the calculated value of β becomes larger.

We now define for non-Markovian time series the quantity $\overline{T}$ in an analogous way with the quantity τ_{eff} introduced above for the Markovian ones, i.e., $1/\overline{T} \equiv 1/\overline{T_h} + 1/\overline{T_l}$, where $\overline{T_h}$ and $\overline{T_l}$ denote the average dwell time in the "high" and the "low" state, respectively. The values of $\overline{T}$ for all SES activities and "artificial" noises mentioned in Fig. 2.8 (which are non-Markovian, e.g., see § 4.1.2) can be found in table I of Ref. [28] and vary in the range from 4 s to 20 s. In Fig. 4.4(a), we give examples of DFA plots of three Markovian time series with $\tau_{low}/2 = \tau_{high}/2 = \tau_{eff} = 4$ s, 10 s and 100 s; the first two ($\tau_{eff} = 4$ s and $\tau_{eff} = 10$ s, upper two curves) have been intentionally selected to have τ_{eff} comparable to the $\overline{T}$ of the SES activities and "artificial" noises. Comparing the DFA plots of the SES activities (that will be discussed later in § 4.4.1) with the upper two curves of Fig. 4.4(a), we find that a cross-over occurs at the *same* region $\Delta t \approx 30$ s (with almost the *same* α exponents in the short scales *only*). In other words, in short time-scales, even Markovian dichotomous time series (that have τ_{eff} values comparable to $\overline{T}$ of the SES activities and "artificial" noises) result in α values in the range $1 \leq \alpha \leq 1.5$ with a cross-over at $\Delta t \approx 30$ s. More generally, we can state [33] that not only signals of dichotomous nature, but *any signal* with a high frequency spectrum as given in Eq. (4.11) will lead to the *same* scaling behavior of $F_{DFA}(\Delta t)$ for small time lags Δt (irrespective of the particular shape of the signal; for example, a Gaussian signal with this spectrum will be much smoother and will display a continuity of values rather than only two steps).

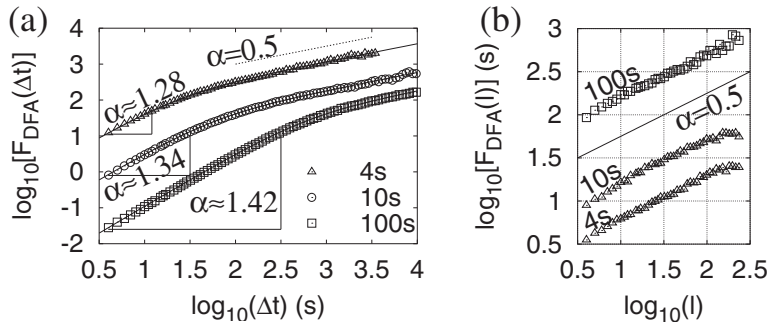

Fig. 4.4 (a) The variability measure $F_{DFA}(\Delta t)$ (in units of ΔE) for three Markovian dichotomous time series, calculated with $\tau_{eff} = 4$ (triangles), 10 (open circles) and 100 s (open squares). The solid lines, in each case, correspond to the theoretical analysis described in § 4.1.3. (b) The same as in (a), but calculated when the time series are read in natural time. The straight lines (dotted in (a), solid in (b)) correspond to $\alpha = 0.5$. The curves are shifted relative to each other by constant factors. Taken from Ref. [33].

The aforementioned points hold provided that the analysis is made in the conventional time frame. If the analysis is performed in natural time (considering as "high" either of the two states in the Markovian series), we find the following values: DFA exponent $\alpha = 0.5$ (see Fig. 4.4(b)) and power spectrum exponent $\beta = 0$. The latter values may elucidate the Markovian nature of the time series, avoiding the existence of the aforementioned characteristic intermediate scaling regions that appear in the analysis in the conventional time frame.

We now turn to the *case of spikes*. This corresponds to a very small value of τ_{eff} ($\approx \tau_{high} \ll \tau_{low}$). Recall that upon decreasing τ_{eff} (see Figs. 4.3(a) and 4.4(a)) the region described by the exponent $\alpha = 0.5$ extends to even shorter scales. This reveals that signals with superposed random spikes exhibit *uncorrelated* behavior (i.e.,$\alpha = 0.5$) at *small* scales.

By summarizing, we can state that:

For Markovian dichotomous signals, the quantity τ_{eff} – defined by $1/\tau_{eff} \equiv 1/\tau_{high} + 1/\tau_{low}$ – plays a key role. For time-scales comparable to (or shorter than) τ_{eff}, the power spectrum can be well described by a power law, $S(f) \propto 1/f^{\beta}$, with an exponent β around unity or larger, for example, $\beta = 1.0$–1.2 (note that β approaches the value 2 and 0 for short and long time-scales, i.e., in the "high"- and "low"-frequencies, respectively). In other words, this reflects that even randomly distributed square pulses could also be approximated by such a behavior. Thus, several published claims that "the appearance of a power law with an exponent β around unity constitutes a signature for critical behavior" should be examined, in each case, with extreme care.

Concerning DFA, a signal with (true) long-range correlations can be misinterpreted as having uncorrelated behavior and vice versa. Specifically: (a) truly correlated signals ($0.5 < \alpha \leq 1.5$) with superposed random spikes may show uncorrelated behavior ($\alpha = 0.5$) at short time-scales, (b) truly uncorrelated signals with superposed random square pulses, show "correlated" behavior (e.g., $\alpha \approx 1.0$–1.4) at time-scales comparable to (or shorter than) τ_{eff}. We can overcome *both* difficulties *if* the analysis is made in natural time.

4.2 Normalized power spectrum of SES activities. The universality emerged in natural time

4.2.1 Normalized power spectrum of SES activities and "artificial" noises in natural time. A universality for SES activities

Figure 4.5(a) depicts the SES activities recorded before the mainshocks labeled K, E and A of Fig. 4.5(b) (excerpts of these SES activities have been shown in Figs. 2.8 and 4.2). Once a SES activity has been recorded, we can read it in natural time and then proceed to its analysis. As an example, let us consider the SES activity K1 (see Fig. 4.5; see also Fig. 1.11(a)) recorded on April 18, 1995, that preceded the M_w6.6 earthquake that occurred

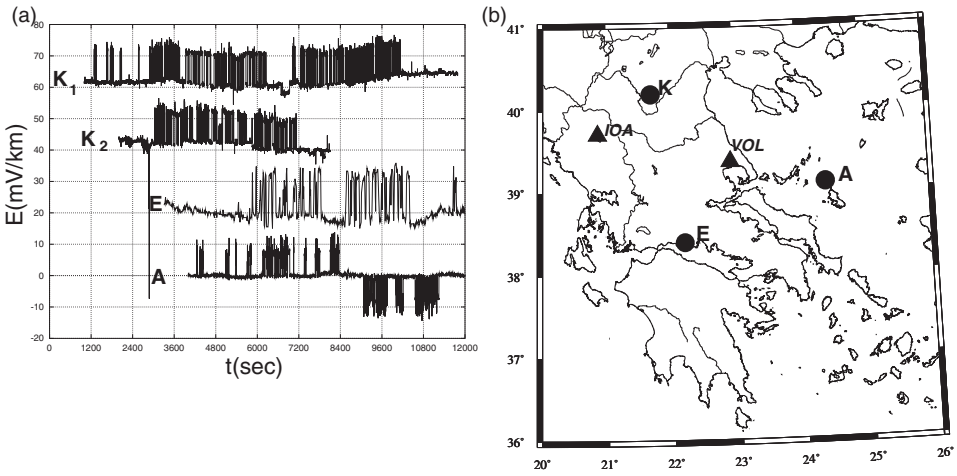

Fig. 4.5 (a) SES activities recorded before the mainshocks on May 13, 1995, (K), June 15, 1995, (E), and July 26, 2001, (A), discussed in § 7.2.1, § 7.2.2 and § 7.2.3, respectively. K1 and K2 refer to the two SES activities before the EQ labeled K (they are also depicted in Fig. 1.11(a),(b)). The upper two SES activities were recorded at IOA, while the lower two at VOL (note that the SES polarities, for drawing convenience, are *arbitrary* here; the correct polarities can be found, for example, in Fig. 4.2). (b) Map showing the EQ epicenters (circles) and the sites (triangles) of the measuring SES stations. Taken from Ref. [31].

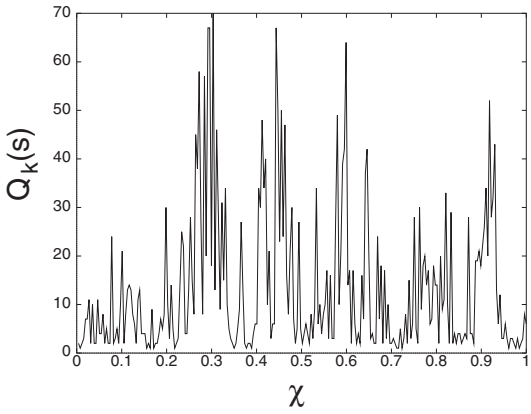

Fig. 4.6 How the SES activity K1 mentioned in Fig. 4.2 (see also Fig. 1.11(a)) is read in natural time; it depicts the durations Q_k as function of the natural time $\chi(=\chi_k)$ but drawn with continuous lines for the convenience of the reader (in reality, this should be plotted as in the lower part of Fig. 2.1(a) or as in Fig. 7.2(b)). Taken from Ref. [32].

at Grevena-Kozani on May 13, 1995 (see § 7.2.1). This lasted for around three and a half hours and was collected with a sampling rate $f_{exp} = 1$ sample/sec (thus we have $N =$ 11,900 data points). Figure 4.6 shows how the SES activity K1 of Fig. 4.5 can be read in natural time.

Figure 4.7 depicts $\Pi(\phi)$ for the four SES activities of Fig. 4.5, along with eight "artificial" noises recorded at various stations of the telemetric network which have a similar feature with SES (but do not satisfy the SES recognition criteria; see Section 1.2).

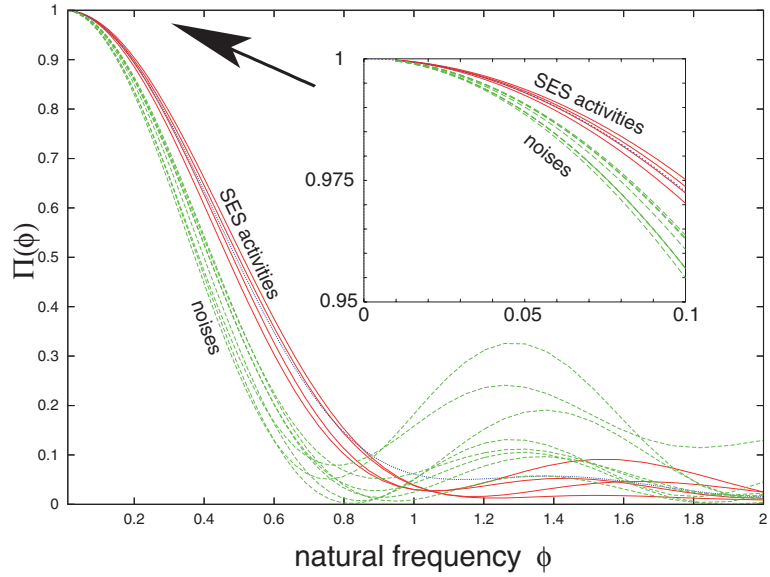

Fig. 4.7 The normalized power spectra $\Pi(\phi)$ for the SES activities (red solid lines) – depicted in Fig. 4.5 – related with the EQs labeled: K, E, and A (in the inset, from the top to the bottom: K1, A, E, K2) along with those of a number of "artificial" noises (green broken lines). The blue dotted curve corresponds to the theoretical estimation of Eq. (2.75), which holds for *critical* dynamics. The inset shows in an expanded scale the behavior of $\Pi(\phi)$ at small ϕ values, i.e., $\phi \to 0$. Taken from Ref. [31].

An inspection of this figure shows the following two facts [31]. First, the curves fall practically into two different classes, labeled "noises" and "SES activities" respectively. This classification, provides a tool for a distinction between "artificial" noises and SES activities (see § 4.2.2).

Secondly, Fig. 4.7 reveals that, for natural frequencies ϕ smaller than 0.5, the $\Pi(\phi)$ values of the SES activities scatter around the dotted curve, which has been estimated from theoretical considerations when approaching a critical point, i.e., Eq. (2.75) of § 2.4.2. In other words, the normalized power spectra in natural time of *all* the SES activities obey a *"universal"* curve.

Note that a possible explanation of the very pronounced "modes" in some "artificial" noises depicted in Fig. 4.7 has been discussed in Ref. [34].

4.2.2 Distinction of SES activities from "artificial" noises based on the normalized power spectrum

Figure 4.8 depicts, for the region of natural frequencies $0 \leq \phi \leq 0.5$, the normalized power spectra $\Pi(\phi)$ of the electric signals mentioned in Fig. 2.8 together with the one corresponding to the "open" states of ICFMC (see Fig. 4.1). The natural time representation of all these electric signals is shown in Fig. 4.9.

Figure 4.8 shows that the curves for the SES activities and "artificial" noises fall practically into two different classes, as already mentioned above (§ 4.2.1), while the ICFMC curve lies just between them and very close to the one that corresponds to the "uniform" distribution (labeled "uniform" in Fig. 4.8); see § 2.1.3. The universal curve for SES activities obeying Eq. (2.75) – which is labeled "theory" in Fig. 4.8 – implies that the variance of χ is $\kappa_1 = \langle \chi^2 \rangle - \langle \chi \rangle^2 = 0.070$ for SES activities (cf. Eq. (2.77), see also the last column in Table 4.1). The κ_1 value that reproduces [32] the ICFMC data is 0.080 ± 0.003 and

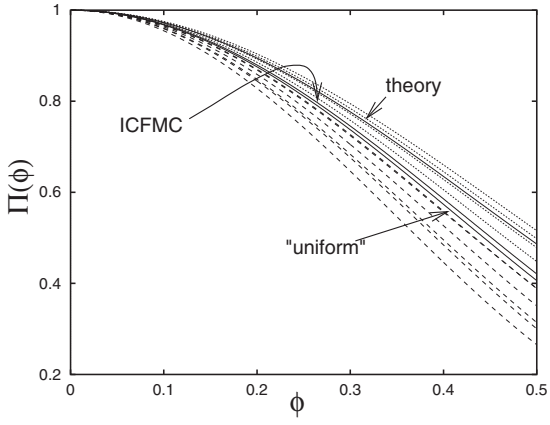

Fig. 4.8 The normalized power spectra $\Pi(\phi)$: SES activities (dotted lines) and "artificial" noises (broken lines) of Fig. 2.8. Three solid curves are also shown: the lower corresponds to the "uniform" distribution (Eq. (2.51) of § 2.4.1), the middle to ICFMC "open" states (see Fig. 4.1 of § 4.1.1), while the uppermost to the theoretical estimation, Eq. (2.75), for SES activities (*critical* dynamics). Reprinted from Ref. [27], Copyright (2009), with permission from TerraPub.

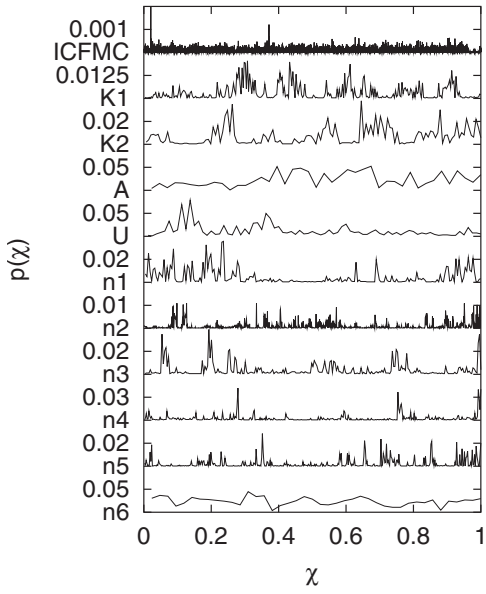

Fig. 4.9 The signals mentioned in Fig. 4.8 read in natural time; it depicts p_k versus χ_k with continuous lines for the sake of reader's convenience and hence $p(\chi)$ versus χ; see Eq. (2.4) (in reality, this should be plotted as in the lower part of Fig. 2.1(a) or as in Fig. 7.2(b)). Taken from Ref. [33]. Excerpts of these signals in the conventional time domain are depicted in Figs. 2.8, 4.1 and 4.2.

$\kappa_u = 1/12 \approx 0.083$ for the "uniform" distribution; see Eq. (2.46). Thus, for the "artificial" noises the variance κ_1 is larger than around 0.083. Hence, the difference $1/12 - \kappa_1 (\equiv \Delta\kappa)$ could be considered as a measure of the deviation of a signal from that of the "uniform" distribution.

By summarizing, SES activities are distinguished from "artificial" noises (AN) according to:

$$\kappa_{1,\mathrm{SES}} < \kappa_u \leq \kappa_{1,\mathrm{AN}} \tag{4.14}$$

where the subscripts designate each class of signals and $\kappa_u \approx 0.083$. Moreover, the SES activities satisfy Eq. (2.77), i.e.,

$$\kappa_{1,\mathrm{SES}} \approx 0.070 \tag{4.15}$$

4.3 Superiority of applying Hurst (R/S) analysis in the natural time domain

4.3.1 Conventional Hurst analysis

A way of studying correlations in a time series is provided by the Hurst analysis [13] known as rescaled range analysis (R/S). This compares the correlations in the time series measured at different time-scales and is similar to the classical fluctuation analysis (FA).

Table 4.1 Summary of the DFA results (when employing E-approximation together with the modification of Eq. (4.20), see § 4.5.2) for the "high"- and the "low"-level states' durations (labeled α_{high} and α_{low}, respectively) along with the κ_1 values for the SES activities and "artificial" noises depicted in Fig. 4.2. Taken from Ref. [34].

Signal	α_{high}	α_{low}	κ_1
K1	0.98±0.08	0.31±0.12	0.063±0.003
K2	0.92±0.10	0.49±0.09	0.078±0.004
A	0.87±0.27	0.34±0.25	0.068±0.004
U	0.98±0.13	0.70±0.15	0.071±0.004
N1	0.68±0.07	0.70±0.08	0.115±0.003
N2	0.79±0.03	0.54±0.04	0.093±0.003
N3	0.78±0.06	0.47±0.08	0.100±0.008
N4	0.76±0.06	0.55±0.06	0.100±0.013
N5	0.68±0.05	0.62±0.05	0.086±0.007
N6	–*)	–*)	0.092±0.004
N7	–*)	–*)	0.083±0.006
N8	–*)	–*)	0.102±0.004
N9	0.78±0.20	0.11±0.20	0.084±0.004

*) For N6, N7 and N8 no reliable slope could be determined in view of the small number of pulses ($N < 25$).

Hurst's method fails to determine correlation properties if linear or higher order trends are present in the data, while detrended fluctuation analysis (DFA) (see § 1.4.2) – which is a significant improvement of FA – explicitly deals with monotonous [5] trends in a detrending procedure with remarkable results.

In short (e.g. see Ref. [5]), in Hurst (R/S) analysis, one calculates in each segment n the range R of the 'profile' $y(n)$ (see Eq. (1.9)) given by the difference between maximal and minimal value $\mathrm{R} = \max[y(n)] - \min[y(n)]$. The 'rescaling of range' is done by dividing R by the corresponding standard deviation S of the same segment. The mean $\langle \mathrm{R/S} \rangle$ of all quotients at a particular scale s is analogous to the fluctuation function $F(s)$ already discussed in the description of DFA (see Eq. (1.12)) and for long-range correlated signals shows a power law scaling relationship with s, with an exponent usually called Hurst exponent H (recall Eq. (2.78)). We first note that *"persistence"* usually means the tendency to keep moving in a fixed direction once the random walker has *started* moving in that direction [47].

In a persistent time series the increase in the values of the series is more likely to be followed by an increase and conversely, the decrease is more likely to be followed by a decrease. This occurs when $1/2 < H < 1$.

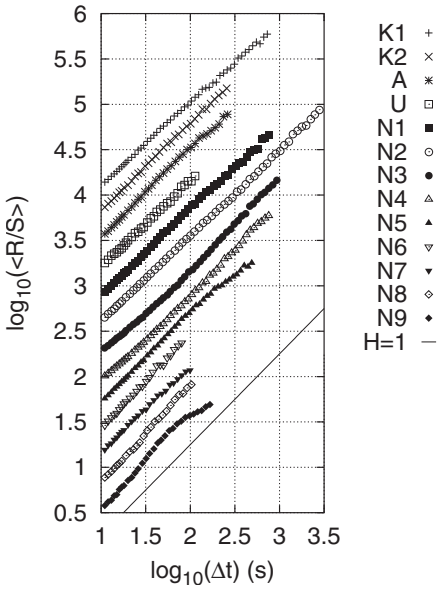

Fig. 4.10 The mean rescaled range $\langle R/S \rangle$ of the Hurst analysis as a function of Δt for the original time series of the SES activities and "artificial" noises mentioned in Fig. 4.2. For the convenience of the reader, the data points for each time series are vertically displaced after subsequent multiplication by a factor of 2, starting from N9; a solid straight line corresponding to $H = 1$ is also plotted. Taken from Ref. [29].

The results of the (R/S) analysis are given in Fig. 4.10 for the original time series of both the SES activities (the upper four curves) and "artificial" noises mentioned in Fig. 4.2. Since $\langle R/S \rangle \propto (\Delta t)^H$, the value of the Hurst exponent H is found from the slope (labeled H_0 in Table 4.2) of the corresponding log-log plot, when approximating it with a single straight line (note that *all* scaling methods related to the original Hurst analysis that yield the H exponent, assume a *finite* variance and according to the central limit theorem the underlying statistics are *Gaussian*).

An inspection of Fig. 4.10 shows that a value in the range $0 < H < 1/2$ (which means *antipersistent* time series, reflecting that increases in the values of a time series are likely to be followed by decreases, and conversely) cannot be seen.

Furthermore, no case with $H = 1/2$ (purely random changes) can be recognized. In all the cases of Fig. 4.10, the resulting H values lie between approximately 0.9 and 1.0 (Table 4.2), which suggest the *persistent* character of the examined time series (strong memory; see Ref. [32] and references therein). Thus, when Hurst analysis is carried out in the original time series, the H values alone cannot lead to any distinction between SES activities and "artificial" noises.

If we repeat the analysis of Fig. 4.10, but for the *dichotomous* time series (i.e., the converted from the original time series "0–1" dichotomous representation) we find somewhat smaller values (labeled H_d in Table 4.2) approximately in the range 0.75 to 0.90. Thus, the conclusion for the persistent character of the time series still remains.

Table 4.2 Summary of the (R/S) analysis for all the signals mentioned in Fig. 4.2. The symbols H_o and H_d stand for the slopes determined by using either the original time series or the dichotomous representation, respectively. H_{high} and H_{low} stand for the corresponding slopes for the "high"- and the "low"-level states' durations, respectively. Taken from Ref. [34].

Signal	H_o	H_d	H_{high}	H_{low}
K1	0.90±0.02	0.77±0.04	0.85±0.05	0.62±0.05
K2	0.96±0.01	0.81±0.05	0.87±0.09	0.70±0.08
A	0.96±0.02	0.76±0.06	0.82±0.28	0.61±0.21
U	0.95±0.02	0.80±0.06	0.89±0.13	0.72±0.12
N1	0.94±0.01	0.78±0.05	0.70±0.07	0.64±0.06
N2	0.94±0.01	0.84±0.04	0.77±0.03	0.58±0.03
N3	0.97±0.03	0.85±0.04	0.80±0.06	0.57±0.05
N4	0.99±0.03	0.87±0.05	0.72±0.04	0.63±0.04
N5	0.94±0.04	0.79±0.06	0.76±0.04	0.66±0.04
N6	1.06*)±0.02	0.86±0.06	–**)	–**)
N7	0.93±0.02	0.79±0.05	–**)	–**)
N8	1.09*)±0.02	0.86±0.05	–**)	–**)
N9	1.01*)±0.20	0.84±0.25	0.75±0.20	0.55±0.22

*) The value of H should *not* exceed unity (see the text), but here we reproduce the directly computed slope. Note that the computed H_d in the third column never exceeds unity.
**) For N6, N7 and N8 no reliable slope could be determined in view of the small number of pulses ($N < 25$).

By summarizing, the (R/S) Hurst analysis of the SES activities and "artificial" noises reveals a *persistent* character of both time series, but *cannot* distinguish between them.

4.3.2 Hurst analysis of the time series of durations of the "high"- and the "low"-level states. Hurst analysis in natural time

The results of Hurst analysis for the time series of durations of the "high"- and the "low"-level states are shown in Fig. 4.11. The analysis of the former states constitutes, of course, the Hurst analysis in natural time (recall Fig. 2.1(a)). The following common characteristic results for *both* the SES activities and "artificial" noises. The H values are systematically larger for the time series of the "high"-level states' durations when compared to the corresponding values of the "low"-level ones (labeled H_{high} and H_{low}, respectively, in Table 4.2). The *persistent* character ($1/2 < H < 1$) of the time series of the "high"-level states' durations seems to be well-established, while this holds to a lesser degree for the time series of the "low"-level ones (because a few of the corresponding H values, e.g. see A, N3 and N9 in Table 4.2, do not differ significantly from 1/2). Moreover in all cases, H_{high} is greater than H_{low}.

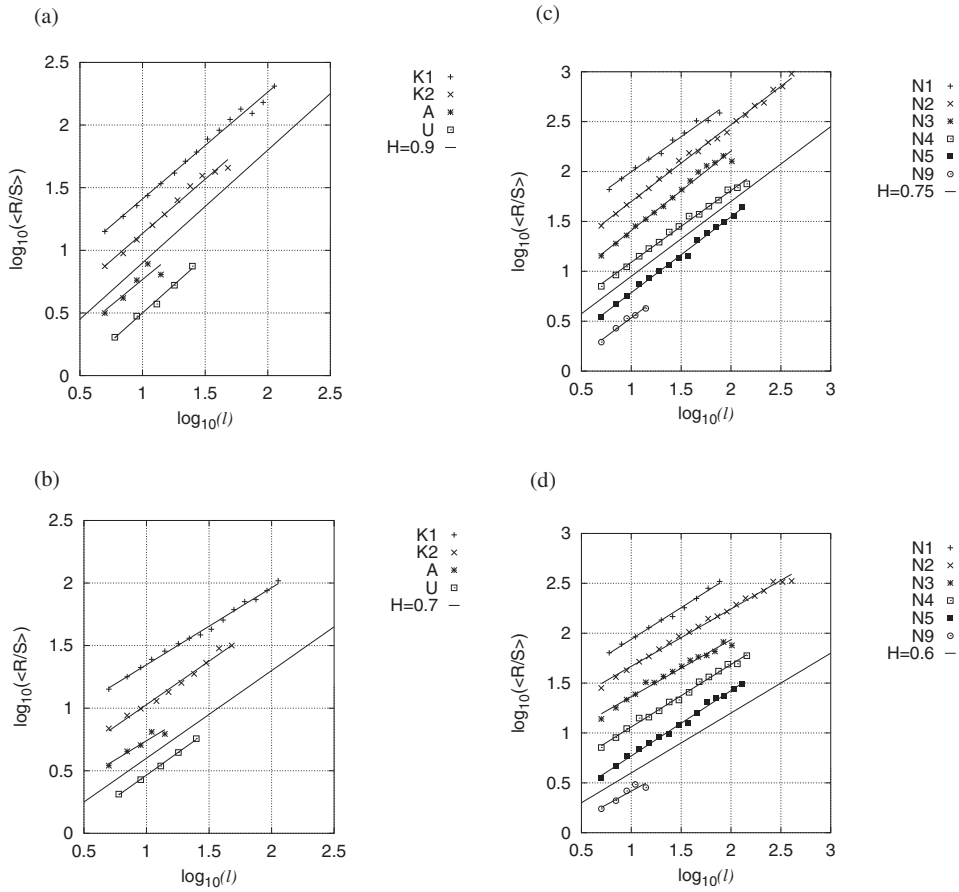

Fig. 4.11 The (R/S) Hurst analysis for the time series of the "high"(panels a and c)- and the "low"(panels b and d)-level states' durations for the SES activities and the "artificial" noises mentioned in Fig. 4.2. The data points for each time series are vertically displaced after subsequent multiplication by a factor of 2, starting from U or N9. For the reader's convenience, apart from the linear least-squares fits, the straight lines with slopes 0.9 in (a), 0.7 in (b), 0.75 in (c) and 0.6 in (d) are also plotted. Taken from Ref. [29].

Hence, the memory of the time series of both the SES activities and "artificial" noises may be mainly attributed to the strong correlation between the "high"-level states' durations.

Note, however, that when comparing the SES activities and "artificial" noises, the H values of their "high"-level states' durations do not differ significantly enough to guarantee a safe distinction between them.

4.4 Superiority of applying detrended fluctuation analysis (DFA) in the natural time domain

4.4.1 DFA of the original time series

Upon using the conventional DFA (§ 1.4.2), we obtain [34] the results depicted in Fig. 4.12 for *both* the SES activities and "artificial" noises mentioned in Fig. 4.2 (cf. recall that the DFA for a long duration SES activity has been already presented in § 1.4.3, see Fig. 1.17). A least squares fit to a single straight line (despite the fact that the data in some cases obviously deviate from such a scheme, see also below) reveals that the slopes of these log-log plots (labeled α_0 in Table 4.3) scatter for all cases around $\alpha \approx 1$, with a plausible uncertainty around 0.15. This reveals long-range temporal correlations. Upon repeating the analysis for their dichotomous time series, slightly different values for each case were obtained (labeled α_d in Table 4.3), and hence the conclusion concerning the strongly persistent character remains the same.

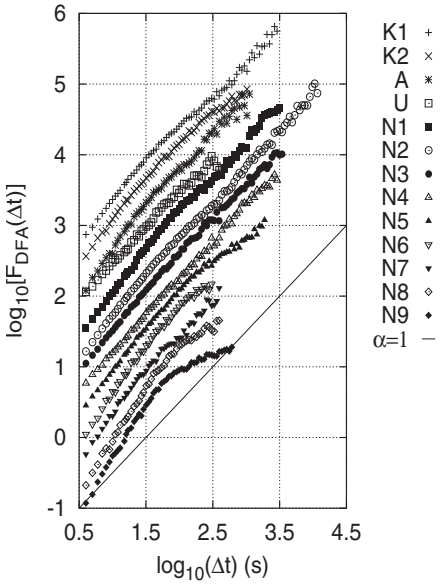

Fig. 4.12 The dependence of F_{DFA} on Δt in the conventional DFA of the original time series (in normalized units) of the SES activities and "artificial" noises mentioned in Fig. 4.2. The data points for each time series are vertically displaced after subsequent multiplication by a factor of 2, starting from N9. For the sake of reader's convenience, a solid straight line corresponding to the slope $\alpha = 1$ is plotted. Taken from Ref. [29].

If the log-log plot in Fig. 4.12 is approximated with two straight lines, the following results were obtained [34]: For *both* SES activities and "artificial" noises, the slope at shorter scales (i.e., $\Delta t \leq 30$ s) was found to lie in the range $\alpha = 1.1$–1.4, labeled α_0^{short} in Table 4.3, while for longer scales a value mostly in the range $\alpha \approx 0.8$–1.0 was determined (labeled α_0^{long} in Table 4.3), without, however, any safe classification between SES activities and "artificial" noises on the basis of the α values alone. The fact that both types of signals exhibit a cross-over at $\Delta t \approx 30$ s and also give almost the same DFA exponent ($\alpha_0^{short} \approx 1.2$)

Table 4.3 Results from the conventional DFA of the signals mentioned in Fig. 4.2. The symbols α_o and α_d stand for the DFA slopes obtained from either the original time series (in normalized units) or the dichotomous representation, respectively, for the whole Δt range. The corresponding slopes when considering either short Δt (smaller than approximately 30 s) or long Δt (larger than approximately 30 s) are also shown, being labeled with a superscript "short" and "long", respectively. Taken from Ref. [34].

Signal	α_o	α_o^{short}	α_o^{long}	α_d	α_d^{short}	α_d^{long}
K1	0.95±0.04	1.19±0.02	0.88±0.02	0.95±0.04	1.21±0.04	0.90±0.02
K2	0.95±0.06	1.22±0.04	0.81±0.02	0.96±0.06	1.23±0.03	0.82±0.02
A	1.06±0.10	1.36±0.05	0.96±0.04	1.08±0.10	1.41±0.05	0.98±0.04
U	0.95±0.04	1.03±0.05	0.81±0.03	0.95±0.04	1.07±0.04	0.79±0.03
N1	1.05±0.05	1.26±0.04	0.98±0.02	1.01±0.05	1.21±0.04	0.95±0.03
N2	1.04±0.03	1.21±0.03	1.01±0.02	0.97±0.03	1.12±0.03	0.94±0.02
N3	1.01±0.04	1.15±0.03	0.97±0.02	0.99±0.04	1.11±0.03	0.95±0.02
N4	1.04±0.04	1.08±0.03	1.02±0.02	1.02±0.04	1.01±0.03	1.02±0.02
N5	0.94±0.10	1.22±0.04	0.79±0.02	0.92±0.10	1.17±0.04	0.78±0.02
N6	1.14±0.11	1.39±0.04	0.89±0.03	1.13±0.11	1.43±0.04	0.86±0.03
N7	1.08±0.09	1.32±0.04	0.96±0.03	1.03±0.09	1.34±0.04	0.82±0.04
N8	1.15±0.12	1.49±0.04	0.78±0.03	1.12±0.12	1.45±0.04	0.76±0.03
N9	0.97±0.20	1.53±0.04	0.55±0.02	0.93±0.20	1.46±0.04	0.52±0.02

can be understood in the context of § 4.1.3 where it is shown that for dichotomous time series such a behavior should be observed at short time scales, i.e., $\Delta t \lesssim \tau_{eff}$.

By summarizing, when the conventional DFA is applied to the original time series of the SES activities and the "artificial" noises, *no* distinction can be achieved.

4.4.2 DFA of the time series of durations of the "high"- and the "low"-level states. Superiority of applying DFA in natural time

We now present the results of DFA for the time series of durations of the "high"- and the "low"- level states which are depicted in Fig. 4.13. Three main points emerge [34]:

First, both the SES activities and "artificial" noises exhibit for the time series of the "high"-level states' durations α values which are systematically larger than the corresponding values of the time series of the "low"-level ones (labeled α_{high} and α_{low}, respectively in Table 4.1).

Second, the α values for the time series of the "high"-level states' durations (which reflects that, *in reality, DFA is applied in natural time*) point to the following difference: for the SES activities (Fig. 4.13(a)) the α_{high} values lie approximately in the range 0.9–1.0, while for the "artificial" noises (Fig. 4.13(c)) the α_{high} values are markedly smaller, i.e., $\alpha_{high} \approx 0.65$–$0.8$ (Table 4.1). We emphasize that such a difference between SES activities and "artificial" noises is *not* noticed upon comparing their series of the "low"-level states' durations.

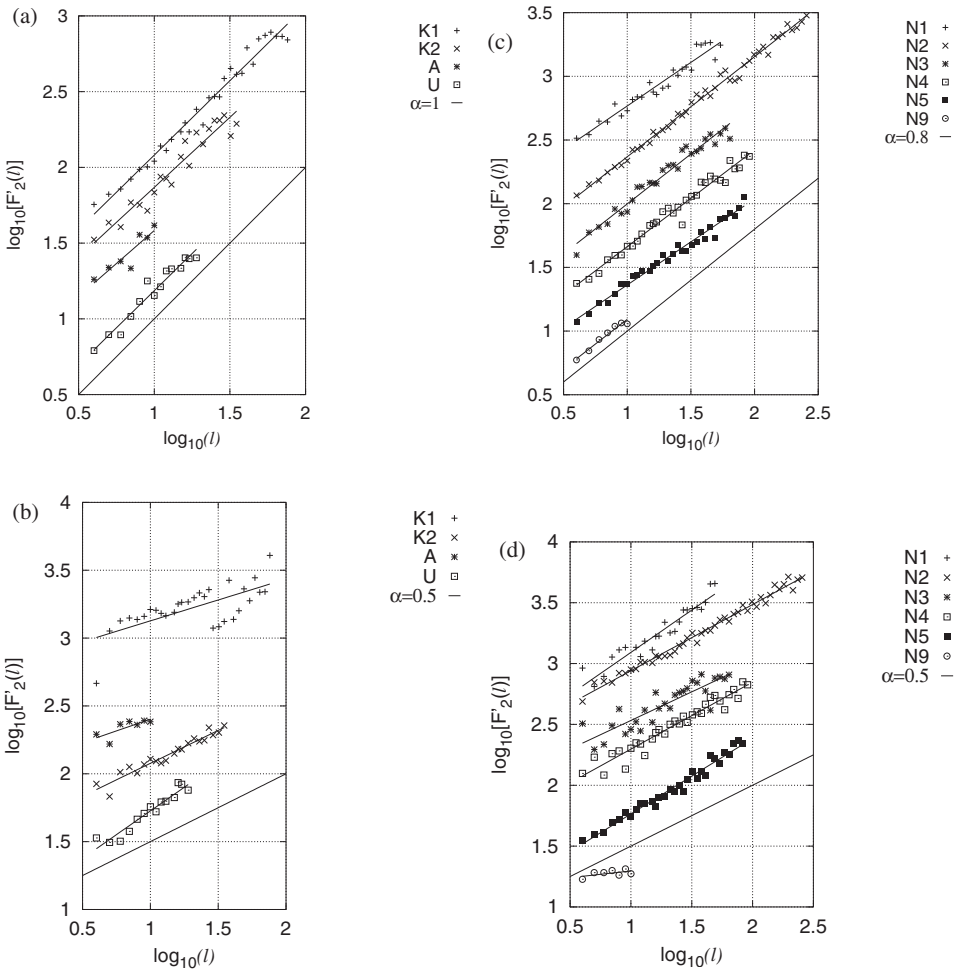

Fig. 4.13 The results of DFA (when employing E-approximation together with the modification of Eq. (4.20); see § 4.5.2) for the time series of the "high" (panels a and c)- and the "low" (panels b and d)-level states' durations (measured in sec, and hence $F_2'(l)$ is also measured in sec) for the SES activities and "artificial" noises mentioned in Fig. 4.2. The data points for each time series are vertically displaced after subsequent multiplication by a factor of 2, starting from U or N9. For the reader's convenience, apart from the linear least-squares fits, the solid straight lines with slopes $\alpha = 1$ in (a), $\alpha = 0.5$ in (b), $\alpha = 0.8$ in (c) and $\alpha = 0.5$ in (d) are also plotted. Taken from Ref. [29].

Third, comparing the α values between the time series of the two states' durations in the SES activities, the following characteristic is found: the α_{low} values for the time series of the "low"-level states' durations scatter more or less around 0.5 (see Fig. 4.13(b)), thus being appreciably smaller than the aforementioned values $\alpha_{high} \approx 0.9$–$1.0$ for the series of the "high"-level states' durations (Fig. 4.13(a)).

Hence, *only* in natural time DFA can distinguish SES activities from "artificial" noises leading to an exponent $\alpha \approx 1.0$ for the SES activities, while $\alpha \approx 0.65$–0.8 for "artificial" noises.

4.5 Superiority of applying multifractal detrended fluctuation analysis (MF-DFA) in the natural time domain

4.5.1 Monofractals and multifractals. The necessity for multifractal analysis

Monofractal signals are *homogeneous* in the sense that they have the same scaling properties, characterized locally by a single singularity exponent h_0, throughout the signal. Thus, monofractal signals can be indexed by a single global exponent, e.g., the Hurst exponent $H \equiv h_0$, which suggests that they are *stationary* from the viewpoint of their local scaling properties (e.g., Ivanov et al. [14] and references therein). Since the power spectrum and the correlation analysis (including the conventional DFA, see § 1.4.2) can measure only one exponent, these methods are more suitable for the investigation of monofractal signals.

Concerning the use of these methods, however, the following points should be considered with care. A power spectrum calculation assumes that the signal is stationary and hence when applied to non-stationary time series it can lead to misleading results, as already mentioned in § 1.4.1. (A time series is stationary if the mean, standard deviation, and all higher moments, as well as the correlation functions, are invariant under time translation.) Thus, a power spectrum analysis should be necessarily preceded by a test for the stationarity of the data analyzed. As for the DFA, see § 1.4.2, it can determine the (mono) fractal scaling properties even in non-stationary time series (but see also Refs. [12, 7] on this point), and can avoid, in principle, spurious detection of correlations that are artifacts of non-stationarities.

In several cases, however, the records cannot be accounted for by a single scaling exponent (i.e., do not exhibit a simple monofractal behavior). In general, if a multitude of scaling exponents is required for a full description of the scaling behavior, a multifractal analysis must be applied. Multifractal signals are intrinsically more complex, and inhomogeneous, than monofractals (e.g., Ref. [14] and references therein). A reliable multifractal analysis can be performed by multifractal detrended fluctuation analysis [46, 15], which is summarized below in § 4.5.2. A similar analysis can be also performed by the wavelet transform (e.g., see Ref. [22]; see also § 4.6.1). Both these methods have been used in Refs. [34, 33] to analyze time series of SES activities and "artificial" noises (for the application of these methods to electrocardiograms see § 9.5.1). It was found [34, 33] that the multifractal analysis, when carried out in the conventional time-frame did not lead to any distinction between these two types of signals, but it *does so*, if the analysis is made in natural time. This will be explained below in § 4.5.3 and § 4.6.2.

4.5.2 Multifractal detrended fluctuation analysis. Background

A generalization of the DFA, termed multifractal DFA (hereafter labeled MF-DFA), allows [46, 15] the multifractal characterization of non-stationary time series. Compared to DFA (see § 1.4.2), in MF-DFA the following additional two steps should be taken.

First, we average over all segments to obtain the q-th order fluctuation function $F_q(s)$:

$$F_q(s) \equiv \left\{ \frac{1}{N_s} \sum_{\nu=1}^{N_s} \left[F^2(s,\nu) \right]^{\frac{q}{2}} \right\}^{\frac{1}{q}} \tag{4.16}$$

where

$$F^2(s,\nu) = \frac{1}{s} \sum_{n=(\nu-1)s+1}^{\nu s} \tilde{y}_s(n)^2, \tag{4.17}$$

and the index variable q can take any real value except zero. This is repeated for several scales s.

Second, we determine the scaling behavior of the fluctuation functions by analyzing log-log plots $F_q(s)$ versus s for each value of q. For long-range correlated series, $F_q(s)$ increases for large values of s as a power law:

$$F_q(s) \propto s^{h(q)}, \tag{4.18}$$

where the function $h(q)$ is called *generalized Hurst exponent*.

For *stationary* time series the aforementioned Hurst exponent H (see § 4.3.1) is identical to $h(2)$,

$$h(2) = H. \tag{4.19}$$

For *monofractal* time series, $h(q)$ is independent of q; all *stationary* long-range correlated series can be characterized by the power law decay of their power spectra $S(f) = f^{-\beta}$ with frequency f, and $\beta = 2H - 1$.

Furthermore, Kantelhardt et al. [16], in order to improve the scaling of the DFA fluctuations at short scales s, suggested a modified fluctuation function using randomly shuffled (*shuf*) copies of the original time series. This modification is useful to be incorporated in MF-DFA as well [15] and can be written as:

$$F_q^{mod}(s) = F_q(s) \frac{\overline{F_q^{shuf}(s')}\ s^{0.5}}{\overline{F_q^{shuf}(s)}\ s'^{0.5}} \tag{4.20}$$

for $s' \gg s$, where $\overline{F_q^{shuf}(s')}$ denotes the root mean square fluctuation function averaged over several configurations of the randomly shuffled data taken from the original record and $s' \approx N/20$.

The MF-DFA method requires series of compact support. In order to analyze data with fractal support, Varotsos et al. [34] suggested an additional modification called "*Eu-*

clidean (E-) approximation". In this approximation, instead of $[F^2(s,\nu)]^{q/2}$ in Eqs. (4.16) and (4.20), the "Euclidean distance" $d(s,\nu) \equiv \{[F^2(s,\nu-1)]^q + [F^2(s,\nu)]^q + [F^2(s,\nu+1)]^q\}^{1/2}$ is used.

In Ref. [34], it was shown that when dealing with time series of small length, *both* the above corrections improve significantly the conventional DFA (see fig. 11 of Ref. [34]). The corresponding fluctuation measure is denoted by $F'_q(s)$ and is the one used in Fig. 4.13 as well as for the determination of $h(q)$ in Figs. 4.14, 4.15 and 4.16.

Relation of MF-DFA to standard multifractal analysis. The scaling exponent $\tau(q)$ in the standard multifractal formalism (§ 4.6.1) is connected to the *partition function* $Z_q(s)$ through

$$Z_q(s) \propto s^{\tau(q)} \tag{4.21}$$

It can be shown [15] that $\tau(q)$ is related to the exponent $h(q)$ defined in Eq. (4.18) as follows:

$$\tau(q) = qh(q) - 1. \tag{4.22}$$

4.5.3 Multifractal detrended fluctuation analysis in natural time compared to that in conventional time

The results of the MF-DFA analysis (§ 4.5.2) of the original time series for both the SES activities and "artificial" noises are depicted in Fig. 4.14. An inspection of this figure shows that no obvious common characteristic can be recognized to allow any systematic distinction between SES activities and "artificial" noises. In order to visualize the difficulty of such a distinction, we reproduce in the inset of Fig. 4.14 a case of a SES activity, i.e., A, which, when compared to the artificial noise N4, shows an almost identical dependence of $h(q)$ versus q (for $q < 4$).

When studying the time series of the durations of the "high"- and the "low"-level states alone (Fig. 4.15), the following common feature emerged. In the time series of the "high"-level states (which reflects – if we recall Fig. 2.1(a) – that, *in reality, MF-DFA is applied in natural time*), the $h(q)$ curves for the SES activities (Fig. 4.15(a)) lie systematically higher than those in the case of "artificial" noises (Fig. 4.15(b)). For example, for $q = 2$, the $h(2)$ values for the SES activities lie close to unity, while for the "artificial" noises they scatter approximately in the range 0.65–0.8 (see Fig. 4.16 and the second column in Table 4.4). On the other hand, if we compare the time series of the "low"-level states' durations (although, in general, they have smaller $h(2)$ values than those corresponding to the "high"-level states' durations), *no* general feature can be recognized to distinguish the SES activities from the "artificial" noises. Varotsos et al. [34] emphasized that the "artificial" noises, which are characterized by $\kappa_1 \geq 0.083$ (§ 4.2.2), are accompanied by $h(2)$ values of the "high"-level states' durations smaller than $\approx$0.8 (see Fig. 4.17). We shall return to this point in § 4.7.1.

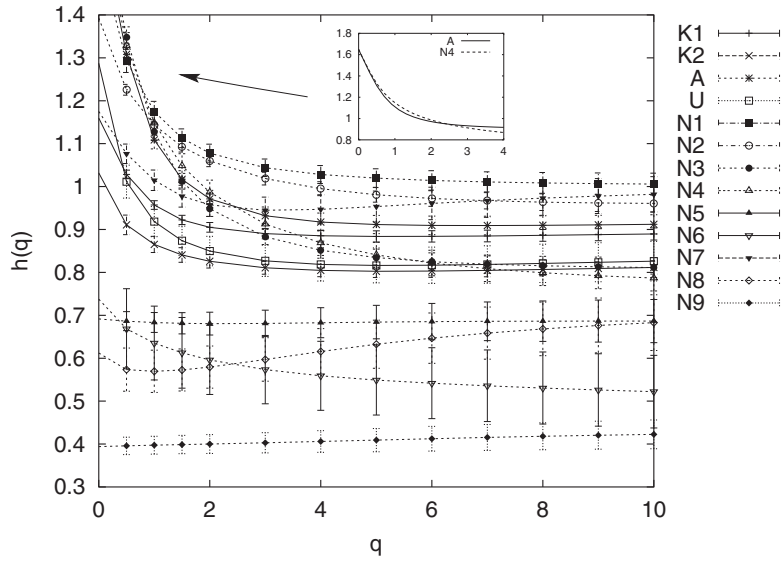

Fig. 4.14 The MF-DFA analysis for the original time series of the SES activities (solid curves) and "artificial" noises (dotted curves) mentioned in Fig. 4.2. The q-dependence of the asymptotic scaling exponent $h(q)$ determined by fits to the log-log plots of $F'_q(s)$ vs s (see § 4.5.2) at the regimes where the fits are straight lines. The corresponding regimes are given in Ref. [29]. For the inset, see the text. Taken from Ref. [29].

Summarizing, when MF-DFA is applied to the original time series of SES activities and "artificial" noises, *no* distinction can be achieved (see Fig. 4.14); *only if* it is applied in natural time can MF-DFA distinguish SES activities from "artificial" noises; see Fig. 4.16 together with the second column in Table 4.4.

4.6 Superiority of applying the wavelet transform in natural time

4.6.1 The wavelet transform, background. Comparison of the estimators of scaling behavior

The main disadvantage of the classical tool of Fourier transform in signal processing is its missing localization property: if a signal changes at a specific time, its transform changes everywhere and a simple inspection of the transformed signal does not reveal the position of the alteration. This originates from the fact that the Fourier transform decomposes a signal in plane waves (trigonometric functions), which oscillate infinitely with the same period and have no local character. Another disadvantage of Fourier analysis lies in the separate description and presentation of time and frequency.

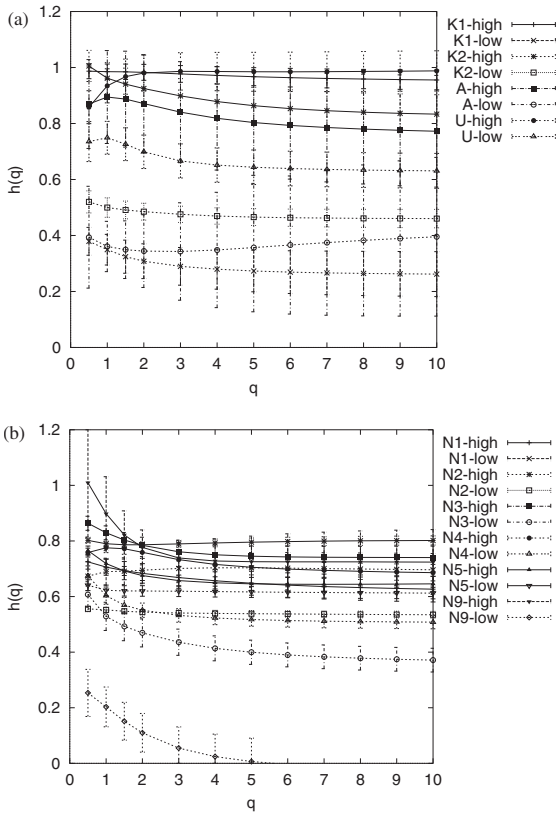

Fig. 4.15 The q-dependence of the asymptotic scaling exponent $h(q)$ obtained from the MF-DFA analysis for the time series of the "high"- and the "low"- level states' durations (labeled high and low, respectively) for: (a) the SES activities and (b) "artificial" noises mentioned in Fig. 4.2. The "high"-level states correspond to the solid lines, and the "low"-level to the dotted lines. Taken from Ref. [29].

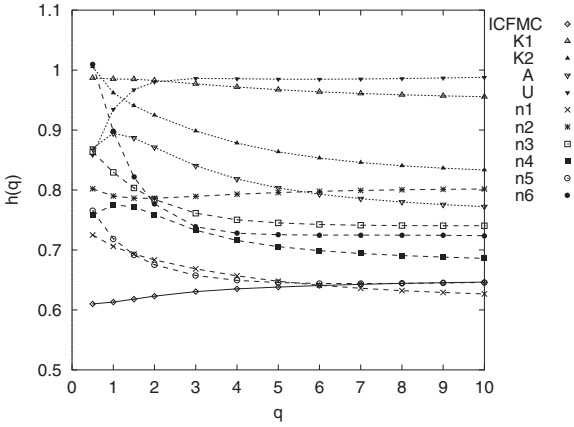

Fig. 4.16 Results of *MF-DFA in natural time* for: the SES activities (dotted lines), "artificial" noises (broken curves) and ICFMC (which corresponds to open states, solid curve). Reprinted from Ref. [27], Copyright (2005), with permission from TerraPub.

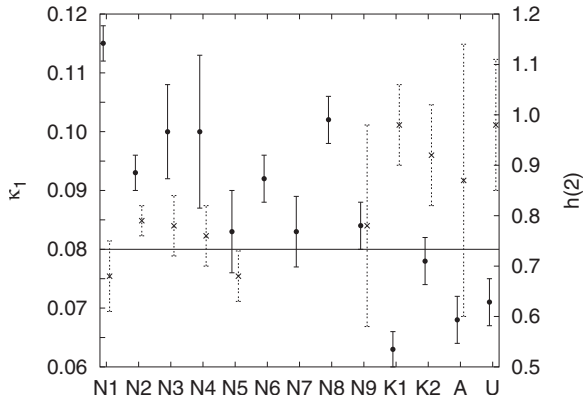

Fig. 4.17 The results of the natural time analysis of the SES activities and the "artificial" noises mentioned in Fig. 4.2. The κ_1 value for ICFMC corresponds to the solid horizontal line at $\kappa_1 = 0.080$. The solid circles correspond to the κ_1 values (left vertical scale). The crosses correspond to the $h(2)$ values (right scale) obtained by MF-DFA (for the noises N6, N7 and N8 no reliable MF-DFA results could be obtained due to the small $N < 25$ number of pulses). Taken from Ref. [34].

Table 4.4 Summary of the results in natural time for the SES activities and the "artificial" noises mentioned in Fig. 4.2 together with the results obtained from the analysis of the closed states for ICFMC. Taken from Ref. [33].

Signal	$h(2)^{*)}$	$h(2)^{**)}$	S	κ_1
K1	0.98±0.08	0.91±0.10	0.067±0.003	0.063±0.003
K2	0.92±0.10	0.94±0.17	0.081±0.003	0.078±0.004
A	0.87±0.27	–	0.070±0.008	0.068±0.004
U	0.98±0.13	1.10±0.27	0.092±0.004	0.071±0.004
ICFMC_c	0.86±0.07		0.096±0.003	0.080±0.003
'uniform'			$\ln(2)/2 - 1/4$	$1/12$
N1 or n1	0.68±0.07	0.86±0.12	0.143±0.003	0.115±0.003
N2 or n2	0.79±0.03	0.81±0.05	0.103±0.003	0.093±0.003
N3 or n3	0.78±0.06	0.69±0.11	0.117±0.010	0.100±0.008
N4 or n4	0.76±0.06	0.84±0.13	0.106±0.010	0.100±0.013
N5 or n5	0.68±0.05	0.77±0.08	0.091±0.011	0.086±0.007
N9 or n6	0.78±0.20	–	0.102±0.007	0.084±0.004

*) From MF-DFA in natural time (§ 4.5.3).
**) From the orthogonal wavelet transform in natural time (§ 4.6.2)

If we use instead a locally confined little wave (*wavelet*), then translation and scaling allows for a "frequency" resolution at arbitrary positions.

Thus, the wavelet transform allows more flexibility (e.g., see Ref. [19]): in simple words, the wavelet, which can be almost any chosen function, can be shifted and dilated to analyze signals. The wavelets can be interpreted as generalized oscillations (small waves) abstractly expressed in a zero mean value (see below). The price of this versatility is that two variables appear in the transform: the location and the scale of the wavelet. If the wavelet ψ is translated to a point t_0 and dilated by a factor l then we calculate the inner (scalar) product of the signal f with the function $\psi_{t_0,l}(t)$. If f shows a big change in a neighborhood of the point t_0 it has a high-frequency spectrum there.

The continuous wavelet transform of a given real function $f(t)$ is defined (e.g., see Ref. [4] and references therein) with a family of test functions $\psi_{t_0,l}(t)$ as the inner product

$$T_\psi[f](t_0,l) = \langle f|\psi_{t_0,l}\rangle \equiv \int f(t)\psi_{t_0,l}(t)\,\mathrm{d}t. \tag{4.23}$$

Each test function $\psi_{t_0,l}$ is obtained from a single function $\psi(t)$ (termed analyzing wavelet) by means of a translation and a dilation:

$$\psi_{t_0,l}(t) = \frac{1}{l}\psi\left(\frac{t-t_0}{l}\right) \tag{4.24}$$

where $t_0 \in \mathscr{R}$ and $l \in \mathscr{R}_+^*$ (where $\mathscr{R}$ stands for the set of real numbers and $\mathscr{R}_+^*$ for the positive ones). The function $\psi(t)$ is chosen such that both its spread in time and frequency are relatively limited.

In addition to being well localized both in time and frequency, ψ is required to satisfy the *admissibility* condition which in its weak form implies that ψ must be of zero mean (hence ψ is a band-pass or oscillating function, whence the name "wavelet", e.g. see Ref. [2] and references therein).

In the study of the scaling behavior, the following two features of the wavelet transform play key roles. (a) The wavelet basis is constructed from the dilation (change of scale) operator; thus the analyzing family exhibits a scale-invariant feature. (b) $\psi(t)$ is chosen so as to have a number $n_\psi \geq 1$ of vanishing moments:

$$\int t^k \psi(t)\,\mathrm{d}t \equiv 0,\ \ k = 0,1,\ldots,n_\psi - 1 \tag{4.25}$$

The Fourier transform $\Psi(\omega)$ of $\phi(t)$ satisfies

$$|\Psi(\omega)| \approx \omega^{n_\psi},\ \ \omega \to 0. \tag{4.26}$$

A common way to build admissible wavelets of arbitrary order n_ψ is to successively differentiate a smoothing function, e.g., the Gaussian function:

$$g_{n_\psi}(t) = \frac{\mathrm{d}^{n_\psi}}{\mathrm{d}t^{n_\psi}}\,\mathrm{e}^{-t^2/2} \tag{4.27}$$

The orthogonal wavelet transform. One can show that if ψ is properly chosen, then the family $\left\{2^{j/2}\psi_{j,k}\right\}_{j,k\in\mathscr{Z}}$, with $\psi_{j,k}(t) = 2^{-j}\psi(2^{-j}t-k)$, is an orthonormal basis of L^2 (e.g., Ref. [19]). The term $2^{j/2}$ is just a normalization factor. The orthogonal wavelet coefficients can then be defined by:

$$d_f(j,k) = \langle f|\psi_{j,k}\rangle. \tag{4.28}$$

Orthogonal wavelets that are often used in practice are the Daubechies wavelets, indexed by a parameter $n_D = 1, 2, \ldots$, which corresponds to the order of the wavelet. The Daubechies wavelet with $n_D = 1$ is in fact the *Haar* wavelet [11] (which is discontinuous; it equals 1 at $0 \leq t < 1/2$, -1 at $1/2 < t \leq 1$ and 0 otherwise), but the Daubechies wavelets with $n_D > 1$ are continuous with bounded support, and have n_D vanishing moments.

The Wavelet Transform Modulus Maxima (WTMM) method. This method [22] is based on the local maxima of the modulus of the continuous wavelet transform, i.e., on the local maxima $t_{0,i}$ (over t_0) of the function $|T_\psi[f](t_0, l)|$, where l is a fixed scale. In other words, in practice, instead of averaging over all values of $|T_\psi[f](t_0, l)|$, one averages (within the WTMM) only the local maxima of $|T_\psi[f](t_0, l)|$ and sums up the q-th power of these maxima,

$$Z(q, l) = \sum_{i=1}^{i_{\max}} |T_\psi[f](t_{0,i}, l)|^q \tag{4.29}$$

If scaling behavior is observed, scaling exponents $\tau(q)$ can be defined by:

$$Z(q, l) \propto l^{\tau(q)} \tag{4.30}$$

These $\tau(q)$ exponents are identical [15] to the τ(q) in Eq. (4.21) and related to $h(q)$ as shown in Eq. (4.22). Attention is drawn to the point that usually in WTMM the time series are analyzed directly instead of the profile $y(i)$ defined in § 1.4.2.

4.6.1.1 Comparison of the estimators of scaling behavior

Most of the (non-parametric) techniques for estimating the scaling exponent of time series that display scaling behavior consist essentially in the measurement of a slope in a log-log plot. Abry et al. [3, 2] and Veitch and Abry [44] have advocated the use of orthogonal wavelet-based estimators, which have several advantages. For example, they are blind to eventual superimposed smooth behavior (such as trends) and they are very robust when changing the slope of the underlying probability law.

Various wavelet-based estimators of self-similarity or long-range dependence scaling exponent were compared by Audit et al. [4]. These estimators mainly include the (bi)orthogonal wavelet estimators and the WTMM estimator. Their study focused both on short and long time series and also compared the wavelet-based estimators with DFA that is not wavelet-based. They found, among others, that the WTMM estimator leads to larger mean squared errors (MSE) for short time series of length smaller than 128 (i.e., $N \leq 128$) as compared to the orthogonal estimators but to much smaller MSE for long time series (see table I of Ref. [4]). For time series of size 8192 (i.e., for sizes comparable to those of the original time series of the SES activities and "artificial" noises), the WTMM estimator using the wavelet g_4, see Eq. (4.27), should be used.

Furthermore, for short time series ($N \leq 128$) it was shown [4] that DFA is the best estimator. This justifies why in § 4.4.2 (as well as in Chapter 5) the method of DFA is employed in order to analyze in natural time the SES activities and "artificial" noises which have usually $N \approx 10^2$ pulses (events).

4.6.2 The wavelet-based methods of estimating scaling behavior in natural time compared to that in conventional time

We start with the application of the WTMM method to the (original) time series of SES activities and "artificial" noises mentioned in Fig. 2.8 (see also the caption of Fig. 4.2). Using a g_4 wavelet, see Eq. (4.27), the analysis led to the results shown in Fig. 4.18. Figure 4.18(b) reveals that the curves showing the q dependence of the generalized Hurst exponent $h(q)$ are not classified, thus not allowing any obvious distinction between SES activities and "artificial" noises. The same conclusion is drawn (see Fig. 4.19(a)) if we apply the orthogonal wavelet transform analysis to the original time series of the signals mentioned in Fig. 2.8. This analysis was made with the program provided by Veitch et al. [45] using the Daubechies wavelet $n_D = 1$, after checking several other Daubechies wavelets of higher order, i.e., $n_D > 1$.

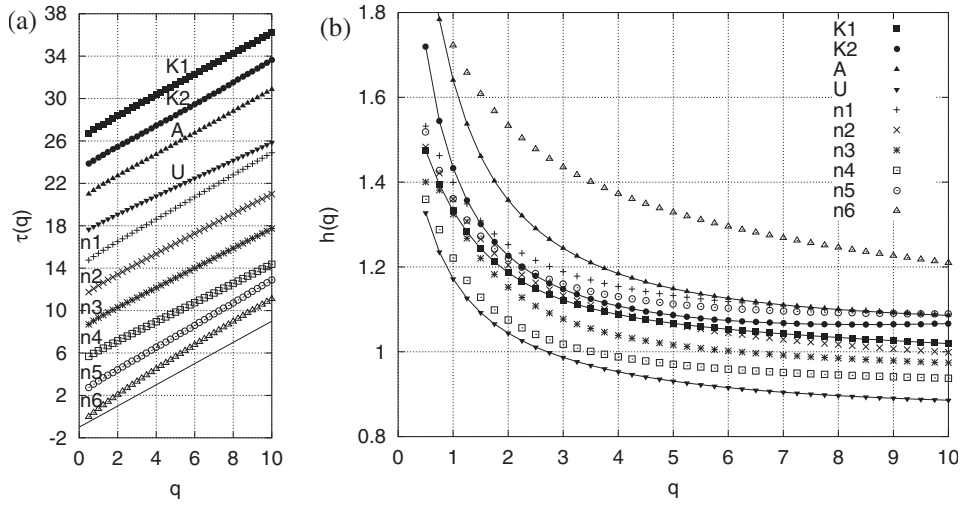

Fig. 4.18 The q dependence of the exponent $\tau(q)$ and the generalized Hurst exponent $h(q)$ (panels a and b, respectively) resulting from the application of WTMM using a g_4 wavelet for the signals mentioned in Fig. 2.8 (see also the caption of Fig. 4.2). For the sake of clarity, the straight line corresponding to a slope $H = 1$ was drawn in (a), while the solid curves in (b) correspond to the four SES activities (bold symbols, while for the "artificial" noises thinner symbols were used). The data points in (a) for each time series are vertically displaced by constant factors. Taken from Ref. [33].

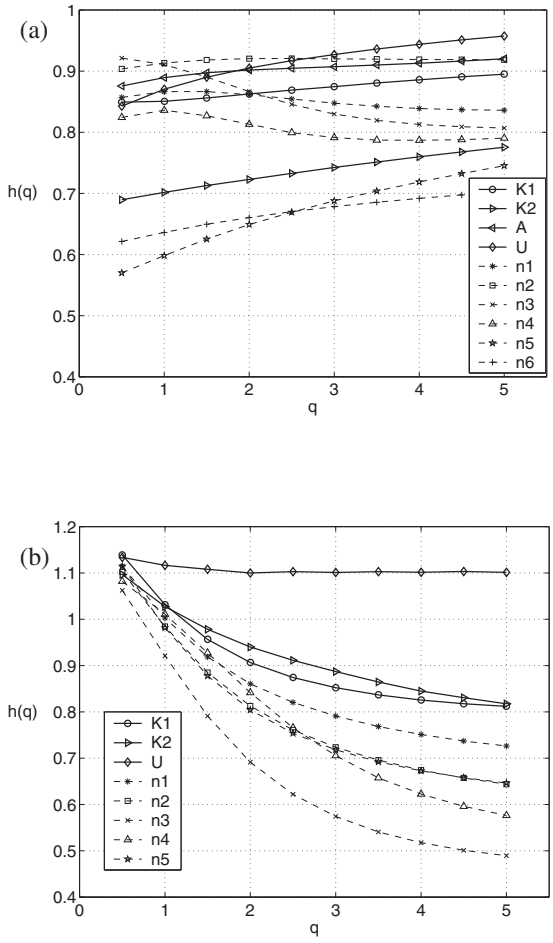

Fig. 4.19 The q dependence of the generalized Hurst exponent $h(q)$ resulting from the orthogonal wavelet transform analysis using a Daubechies1 (i.e., $n_D = 1$) wavelet. The solid curves correspond to the SES activities while the broken to the "artificial" noises: (a) of the original time series mentioned in Fig. 2.8 (see also the caption of Fig. 4.2); the percentage errors in the determination of h(2) are: 5, 15, 8, 4, 6, 3, 4, 12, 19 and 15% for K1, K2, A, U, n1, n2, n3, n4, n5, and n6 respectively.(b) of the time series read in natural time, see Fig. 4.9 (the corresponding errors are presented in Table 4.4); note that the signals A and n6 could not be analyzed in natural time due to the small number of pulses. Taken from Ref. [33].

We now proceed to the application of the wavelet transform to the signals as they are read in natural time, see Fig. 4.9. The results of the orthogonal wavelet transform analysis (note that WTMM could not be reliably applied in view of the small number of pulses), using again the Daubechies $n_D = 1$ (i.e., Haar) wavelet, are depicted in Fig. 4.19(b). An inspection of these $h(q)$ versus q curves, in spite of the large estimation errors seems to show a classification as follows. For q values around 2 or larger the resulting $h(q)$ values for the SES activities are higher than those of the "artificial" noises (see the $h(2)$ values in the third column in Table 4.4). In particular, the results show that the generalized Hurst exponent $h(2)$ for the SES activities is close to unity, while for the "artificial" noises $h(2)$ is markedly smaller. This conclusion is fully compatible with that deduced from the application of MF-DFA in natural time (§ 4.5.3, see also the second column in Table 4.4).

In summary, the wavelet transform analysis allows a distinction between SES activities and "artificial" noises, but *only* if it is applied in natural time leading to $h(2) \approx 1$ for SES activities, while $h(2)$ is markedly smaller for "artificial" noises.

4.7 Combining the normalized power spectrum analysis and multifractal analysis in natural time. The K-means clustering algorithm

4.7.1 Combining the variance κ_1 and the generalized Hurst exponent $h(2)$

Towards this goal, we employ two independent methods: the normalized power spectrum analysis in natural time (leading to the κ_1 values, see § 4.2.2) and the MF-DFA (§ 4.5.3) the application of which in natural time led for $q = 2$ to the $h(2)$ values given in Table 4.4 (see also the columns labeled α_{high} and κ_1 in Table 4.1). Figure 4.20 presents the results for the signals mentioned in Fig. 2.8 (see also the caption of Fig. 4.2) of these two methods applied independently in natural time.

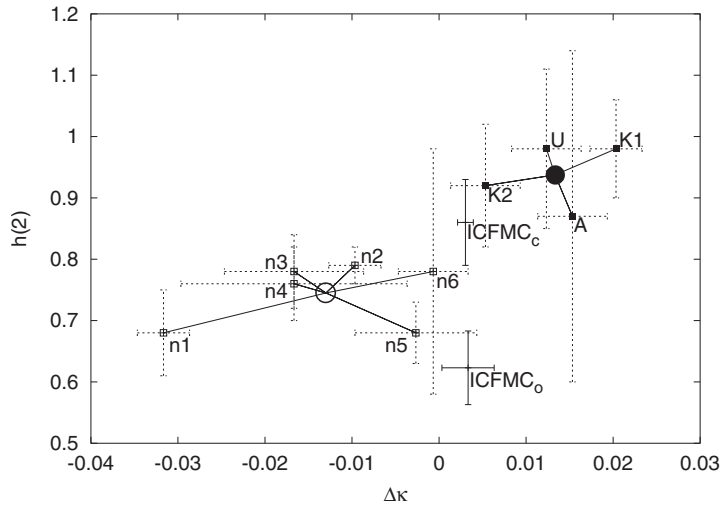

Fig. 4.20 Combined results of the analyses in natural time, see § 4.7.1. Plot of $h(2)$ versus $\Delta\kappa$ (= $1/12 - \kappa_1$): SES activities K1, K2, A, U (filled squares), "artificial" noises n1 to n6 (open squares), and the ICFMC (open states, labeled ICFMC$_o$). The κ_1 values come from the normalized power spectrum analysis (see Fig. 4.8), while the $h(2)$ values were obtained by MF-DFA (Fig. 4.16); all these values are given in Table 4.4. The DFA exponent (≈0.86) of the closed states for ICFMC (labeled ICFMC$_c$) is also inserted [33]. The thick straight lines indicate the two groups resulting from the application of the K-means algorithm explained in § 4.7.2; the full and open circles show the centroids of the two groups. Taken from Ref. [33].

A unified feature seems to emerge. The deviations from the "uniform" behavior quantified by $\Delta\kappa$ (where $\Delta\kappa \equiv 1/12 - \kappa_1$, see § 4.2.2) are interrelated with the $h(2)$ values: First, the SES activities, which correspond to large $\Delta\kappa$ values ($\Delta\kappa > 0$), are characterized by the strongest "memory" (large $h(2)$, close to unity); both their $\Delta\kappa$ and $h(2)$ values are consistent with those expected for a critical behavior (see § 4.7.3 and § 2.4.2). Second, the "artificial" noises simultaneously have smaller $\Delta\kappa$ values ($\Delta\kappa \leq 0$) and weaker "memory" (their $h(2)$ values are markedly smaller than unity). Third, concerning the ICFMC, the values related with the closed states, which have been found [24] to exhibit the stronger "memory" (between the two states, i.e., closed and open, see Fig. 4.1), seem to lie between the aforementioned two regimes.

Finally, Varotsos et al. [33] emphasized that, the randomly "shuffled" series of all the three types of electric signals investigated, lead to $h(2) \approx 0.5$ (simple random behavior) and $\Delta\kappa \approx 0$ (e.g., see the SES activity in § 7.1.1). These two values are internally consistent in the absence of heavy tails, because in the "shuffling" procedure the values are put into random order, thus all correlations (memory) are destroyed (§ 2.5.2.1).

4.7.2 The K-means clustering algorithm

A more elaborated classification of the results depicted in Fig. 4.20, can be obtained by using some clustering algorithm. In Ref. [33] a K-means type was used, which is a least-squares partitioning method allowing users to divide a collection of objects into K groups (e.g., see section 8.8 of Ref. [18]).

The K-means problem consists of dividing a set of multivariate data into non-overlapping groups in such a way as to minimize the sum (across the groups) of the sums of squared residual distances to the group centroid (this statistics is usually called sum of squared errors). In other words, a computer program tries to minimize the sum, over all groups, of the squared within-groups residuals, which are the distances of the objects to the respective group centroid. The groups obtained are such that they are geometrically as compact as possible around their respective centroid.

In Ref. [33] the K-means partitioning program provided by Legendre [17] was used. This program allows users to search through different values of K in a cascade, starting with k_1 groups and ending with k_2 groups, with $k_1 \geq k_2$. In the cascade from a larger to the next smaller number of groups, the two groups whose centroids are the closest in multivariate space are fused and the algorithm iterates again to optimize the sum of squared errors function, reallocating objects to the groups. Varotsos et al. [33] run the program by considering the 10 "objects", i.e., the four SES activities and the six "artificial" noises mentioned in Fig. 2.8 (see also the caption of Fig. 4.2). The $h(2)$ values resulting from MF-DFA in natural time and the κ_1 values reported in Table 4.4 have been used. Studying partitions from $k_1 = 5$ to $k_2 = 2$ groups, the clustering shown in Fig. 4.20 with the thick straight lines was found [33].

This clustering consists of the following two groups ($K = 2$): the first one includes the four SES activities, while the second the six "artificial" noises n1 to n6. The centroid of the first group (solid dot) lies at $\Delta\kappa = 0.013$, $h(2) = 0.9375$, while the centroid of the second at $\Delta\kappa = -0.013$, $h(2) = 0.745$. Note that the $\Delta\kappa$ value ($= 1/12 - \kappa_1$) of the centroid of the group of the four SES activities corresponds to $\kappa_1 = 0.070$, which coincides with the theoretical value obtained for the SES activities in § 2.4.2, see Eq. (2.77).

4.7.3 Comments on the differences in the memory and the variance κ_1 among electric signals of different nature

Let us focus on the tentative origin of the difference in the memory of SES activities and "artificial" noises. In Ref. [34] an attempt was made towards understanding the aforementioned results (§ 4.5.3), which show that the values of the generalized Hurst exponent $h(2)$ of the "high"-level states' durations of the SES activities are close to unity, while those of the "artificial" noises are markedly smaller. Let us consider, at the moment, for the sake of simplicity, the simple case of fBm (which has been proposed [48] to model the SES activities for $H \to 1$ and is the *only* Gaussian self-similar process with self-similarity index $H \neq 0.5$, e.g., see Ref. [21]; see also § 1.5.1.1): the Hurst exponent H has been suggested as a measure of the degree (intensity) of self-similarity or long-range dependence, e.g., see Ref. [26] (see also Refs. [20, 49]). The power law decay of the covariance, Eq. (1.8), characterizes long-range dependence. The higher the H the slower the decay, e.g., see Eq. (1.15). If we now assume that, in general, $h(2)(= H)$ is actually a measure of the intensity of long-range dependence, we may understand that the SES activities, since they exhibit *critical* dynamics (infinite long-ranged correlations), should have a long-range dependence stronger (thus, a higher H) than that of the "artificial" noises. Note that the model of critical behavior discussed in § 2.4.2, which resulted in Eq. (2.77), shows that $\mathscr{E}(Q_k Q_{k+l})$ is independent of l.

As for the fact that the ICFMC curve ($\kappa_1 = 0.080 \pm 0.003$) lies in Fig. 4.8 closer to the "uniform" distribution compared either to the SES activities or the (majority of the) "artificial" noises, this is not unreasonable for a biological system [34] (see Chapter 9, e.g., Fig. 9.11).

4.8 The fluctuation function $F(q) = \langle \chi^q \rangle - \langle \chi \rangle^q$ and the entropy S in natural time

4.8.1 Classification of electric signals based on the function $F(q) = \langle \chi^q \rangle - \langle \chi \rangle^q$ versus q in various types of electric signals

In Ref. [33], it was proposed that a classification of the aforementioned three types of electric signals of dichotomous nature, i.e., ICFMC, SES activities and "artificial" noises,

becomes possible if we study, in the range $0 < q \leq 2$, the function $F(q) = \langle \chi^q \rangle - \langle \chi \rangle^q$ versus q.

We recall that Fig. 4.9 shows how the electric signals, mentioned in Fig. 4.8 (see also Figs. 2.8 and 4.2), are read in natural time. The function $\langle \chi^q \rangle - \langle \chi \rangle^q$ versus q, for all these electric signals, is depicted in Fig. 4.21(a), in the range $0 < q \leq 2$. (cf. Eq. (2.38), which was introduced for $n =$ positive integer only). This figure shows that the signals are now classified:

> The curves for the SES activities and "artificial" noises, at least in the range $q \in (1,2)$ fall practically into two different classes, while the ICFMC curve lies just between them.

Note that the results, for $q = 2$, exhibit the feature already mentioned in § 4.2.2, i.e., for SES activities, they scatter around the value $\kappa_1 (= \langle \chi^2 \rangle - \langle \chi \rangle^2) = 0.070$, while for the "artificial" noises $\kappa_1 \geq 0.083$, and for ICFMC $\kappa_1 = 0.080 \pm 0.003 \approx \kappa_u$ (see also Fig. 4.8).

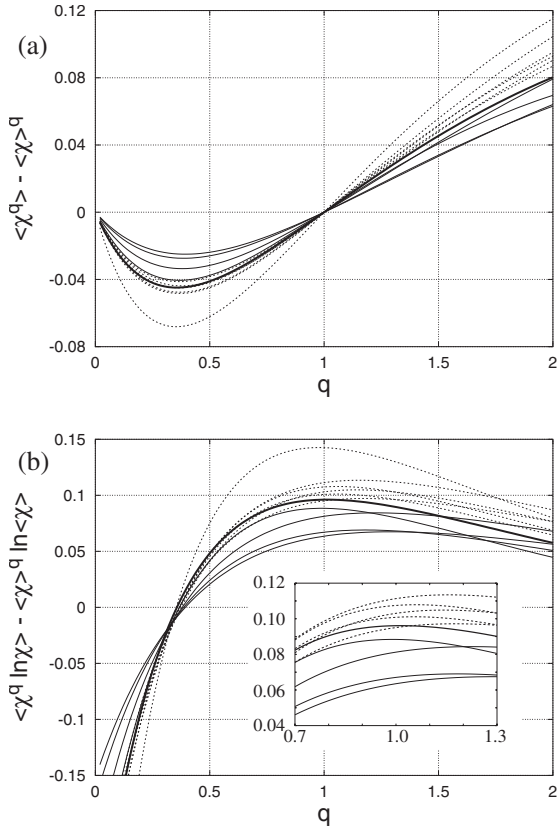

Fig. 4.21 (a) The function $\langle \chi^q \rangle - \langle \chi \rangle^q$ and (b) its derivative with respect to q, i.e., $\langle \chi^q \ln \chi \rangle - \langle \chi \rangle^q \ln \langle \chi \rangle$, versus q. ICFMC: Thick solid line; SES activities: thin solid lines; "artificial" noises: broken lines. The uncertainties for $q = 2$ in (a) and for $q = 1$ in (b) are given in Table 4.4. Taken from Ref. [33].

4.8.2 Classification of electric signals based on the entropy S in natural time

The derivative of the function $F(q) = \langle \chi^q \rangle - \langle \chi \rangle^q$ with respect to q, i.e.,

$$F'(q) = \frac{\mathrm{d}}{\mathrm{d}q} \left(\langle \chi^q \rangle - \langle \chi \rangle^q \right) = \langle \chi^q \ln \chi \rangle - \langle \chi \rangle^q \ln \langle \chi \rangle \tag{4.31}$$

is plotted in Fig. 4.21(b) versus q. We may see again a classification. Furthermore, Varotsos et al. [33] drew attention to the region around $q = 1$. The quantity $\langle \chi \ln \chi \rangle - \langle \chi \rangle \ln \langle \chi \rangle$ is just the one defined as entropy S in natural time, i.e., see Eq. (3.1). In addition, Eq. (3.4) states that the entropy S_u of the "uniform" distribution (see § 2.1.3) has the value $S_u = 0.0966$.

Therefore the three types of electric signals seem to be classified as follows (but see also § 4.8.3): The "artificial" noises have an entropy larger than (or equal to) that of the "uniform" distribution, i.e., $S \geq S_u$, while the SES activities exhibit S values smaller than S_u. As for the ICFMC, the S value lies just in the boundary between the SES activities and the "artificial" noises and is very close to S_u. The point that only n5 among the "artificial" noises seems to have a smaller entropy than S_u – see Table 4.4 – is discussed below.

Thus, in short, the entropy $S = \langle \chi \ln \chi \rangle - \langle \chi \rangle \ln \langle \chi \rangle$ of the SES activities is smaller than that (S_u) of the "uniform" distribution, while the "artificial" noises have an entropy larger than (or equal to) S_u.

The following remarks are worth adding. First, when employing the K-means algorithm mentioned in § 4.7.2, if the S values inserted in Table 4.4 are used instead of κ_1, a comparison of partitions into $k_1 = 4$ to $k_2 = 2$ groups also leads to the clustering shown in Fig. 4.20.

Second, for each of the signals depicted in Fig. 4.9, the values of the scaling exponent α (obtained from DFA) and κ_1 do *not* change upon a time reversal. Such a reversal, however, leads to a different S value labeled S_-.

The latter important point has been already treated in Section 3.4 and will be further discussed in Section 4.9. Third, if the number of pulses in a SES activity (or "artificial" noise) is small (e.g. 3–50), the values of *both* κ_1 and S are *smaller* than the actual ones; the extent of this underestimation could be understood on the basis of Fig. 4.22 to which we now turn. Figure 4.22, depicts the expected value for κ_1 and S for a Markovian dichotomous time series (Section 4.1) as a function of the number of the "high" level states N along with their uncertainty of $\pm\sigma$. Recall that the values of κ_1 and S for all the SES activities and "artificial" noises mentioned in Fig. 4.9, are shown in Table 4.4. The fact that only n5 among the "artificial" noises seems to have an entropy somewhat smaller than S_u ($S[\mathrm{n5}] = 0.091 \pm 0.011$) might be understood as follows: for n5, we have $N \approx 400$ (see Table 2.2) for which Fig. 4.22 reveals that the aforementioned value of 0.091 differs from S_u only by an amount smaller than one σ.

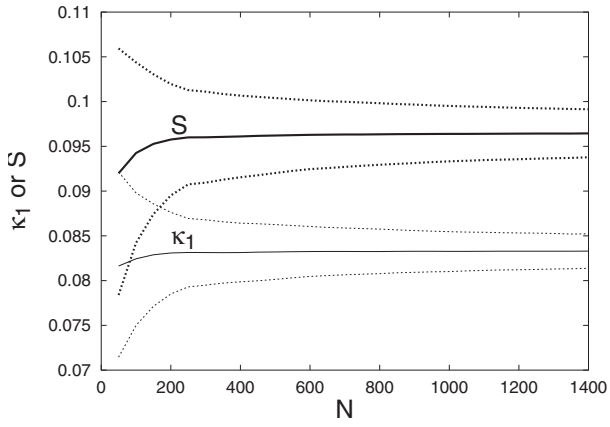

Fig. 4.22 Confidence intervals ($\mu \pm \sigma$) for the variance κ_1 (thin lines) and the entropy S (thick lines) calculated for a Markovian dichotomous time series (note that the durations Q_k are exponentially distributed) versus the number of events N. The solid lines correspond to the average values of κ_1 (thin) and S (thick). Taken from Ref. [28].

4.8.3 Classification of electric signals by the complexity measures using the fluctuations of the entropy in natural time

The values of the complexity measures λ_s, $\lambda_{s,shuf}$ and ν_s, defined in § 3.6.1, for several SES activities and "artificial" noises were calculated in Ref. [38] and the results are shown in Table 4.5. The complexity measures have been calculated only in the short-range because the length of these signals in the natural time domain is on the average $\approx 10^2$ pulses and hence does not significantly exceed the time window length $l \approx 60$ pulses, thus not allowing a reliable calculation of the complexity measures in the longer scale (see § 3.6.1; see also § 9.2.2.1 and § 9.2.7).

Table 4.5 The complexity measures λ_s, $\lambda_{s,shuf}$ and ν_s of SES activities and "artificial" noises along with their S values (note that the latter are compiled from Table 4.4). Taken from Ref. [36].

Signal	λ_s	$\lambda_{s,shuf}$	ν_s	S
K1	1.26	1.27	1.21	0.067±0.003
K2	1.26	1.29	1.30	0.081±0.003
U*)	1.06	1.24	1.17	0.092±0.004*)
A	0.97	1.14	0.97	0.070±0.008
n1	1.25	1.23	1.21	0.143±0.003
n2	1.30	1.31	1.18	0.103±0.003
n3	1.35	1.26	1.24	0.117±0.010
n4	1.36	1.26	1.20	0.106±0.010
n5*)	1.32	1.28	1.12	0.091±0.011*)
n6	1.36	1.01	1.15	0.102±0.007

*) Note that in these two cases the S values are comparable to S_u, and hence their distinction can be made on the basis of the λ_s values which differ markedly.

An inspection of these results reveals that the λ_s values of most "artificial" noises are somewhat *larger* than those in the SES activities. Note that in two cases, i.e., the SES activity U and the "artificial" noise n5, for which the S values are comparable to S_u (thus, no distinction can be made on the basis of the S values alone), the distinction can be achieved on the basis of the λ_s values, $\lambda_s(U) < \lambda_s(n5)$, which differ markedly.

Recapitulating the distinction of similar-looking signals that are emitted from systems of different dynamics, we can now say the following [38]: If the S values differ markedly from S_u (which holds in most SES activities and "artificial" noises), the signals can be distinguished on the basis of the S values alone. On the other hand, if the S values are close to S_u (which holds in all ECG, see Chapter 9, but only in the minority of SES activities and "artificial" noises) the signals can be better classified by using the complexity measures based on the fluctuations δS of the entropy (see also § 3.6.1 and § 9.1.1).

4.9 Using the entropy S_- or the fluctuations of natural time under time reversal

4.9.1 Distinction of SES activities from "artificial" noises based on the entropy in natural time under time reversal

The entropy S_- in natural time under time reversal, defined in § 3.4.1 has been calculated for all the SES activities and "artificial" noises tabulated in Table 4.4 (as well as for some more recent examples) and the results can be found in Ref. [43] (see also Ref. [42]). Here, Table 4.6 compiles the S and S_- values of all these signals along with those of 16 SES activities recorded during the subsequent years. The stations at which the latter SES activities have been recorded are also mentioned in Table 4.6. For the sake of completeness, we also give in Table 4.6, the value of the variance $\kappa_1 = \langle \chi^2 \rangle - \langle \chi \rangle^2$ obtained in each case. An inspection of Table 4.6 reveals the following:

The S values are actually classified, as stated above in § 4.8.2, i.e., $S < S_u$ for the SES activities and $S_u \lesssim S$ for "artificial" noises. On the other hand, this does *not* hold in general for the S_- values.

This is so, since for all the SES activities (with the probable exception of K2) we find that the S_- values are smaller than (or equal to) S_u, but for "artificial" noises no *common* behavior could be found, because S_- is either smaller or larger than S_u.

In other words, no distinction between SES activities and "artificial" noises can be achieved on the basis of S_- values *alone*. This means the following, if we recall that the S value takes into account the sequential order of pulses and hence captures elements of the dynamics hidden in this order [37, 38]: Only when considering the true time arrow (i.e.,

analyzing in natural time the signal as it was actually recorded in nature) the S value can pinpoint the difference in the dynamics between these two groups of electric signals. Recall that the SES activities are characterized by *critical* dynamics and hence exhibit infinitely ranged long-range correlations, while in "artificial" noises the intensity of the long-range correlations is markedly weaker [33] (see also § 4.7.3). Numerical studies of models which show [41] that *both* S and S_- are smaller than S_u have been already presented in § 3.4.3 and § 3.4.4.

Table 4.6 The values of S, κ_1, S_- for the SES activities and "artificial" noises in Greece analyzed in Ref. [43] (see also table I of Ref. [42]) together with the one labeled E in Fig. 4.5 as well as with 16 more recent SES activities which are the following: M_1 to M_4 were recorded at MYT station, while V_1 at VOL, see fig. 1 of Ref. [41]. The SES activities PAT, shown in Fig. 7.2, and PAT_2, see fig. 2 of Ref. [40], were recorded at PAT station. The signals PIR_1, PIR_2, PAT_3 and PAT_4 correspond to the SES activities depicted in figs. 3(a), 3(b), 3(d) and 3(e) of Ref. [39], respectively. They were recorded at PIR or PAT station. The four additional SES activities recorded at PAT station during 2007 depicted in figs.5(a), 5(b), 5(c) and 5(d) in Ref. [30] are labeled PAT_5, PAT_6, PAT_7 and PAT_8, respectively. Finally, PIR_3 stands for the SES activity (see Fig. 7.22(b)) that was recorded [30] on January 14, 2008, at PIR which preceded the strongest earthquake in Greece during the last 28 years that occurred on February 14, 2008.

Signal	S	κ_1	S_-
K1	$0.067\pm0.003^{*)}$	$0.063\pm0.003^{*)}$	0.074 ± 0.003
K2	$0.081\pm0.003^{*)}$	$0.078\pm0.004^{*)}$	0.103 ± 0.003
E	0.071 ± 0.010	0.071 ± 0.006	0.082 ± 0.010
A	$0.070\pm0.008^{*)}$	$0.068\pm0.004^{*)}$	0.084 ± 0.008
U	$0.092\pm0.004^{*)}$	$0.071\pm0.004^{*)}$	0.071 ± 0.004
T1	0.088 ± 0.007	0.084 ± 0.007	0.098 ± 0.010
C1	0.083 ± 0.004	0.074 ± 0.002	0.080 ± 0.004
P1	0.087 ± 0.004	0.075 ± 0.004	0.081 ± 0.004
P2	0.088 ± 0.003	0.071 ± 0.005	0.072 ± 0.015
E1	0.087 ± 0.007	0.077 ± 0.017	0.081 ± 0.007
$M_1^{**)}$	0.094 ± 0.005	0.075 ± 0.004	0.078 ± 0.003
$M_2^{**)}$	0.089 ± 0.003	0.076 ± 0.004	0.084 ± 0.003
$M_3^{**)}$	0.089 ± 0.004	0.080 ± 0.005	0.093 ± 0.004
$M_4^{**)}$	0.080 ± 0.005	0.073 ± 0.004	0.086 ± 0.006
$V_1^{**)}$	0.078 ± 0.006	0.074 ± 0.004	0.092 ± 0.005
$PAT^{***)}$	0.080 ± 0.002	0.072 ± 0.002	0.078 ± 0.002
$PAT_2^{***)}$	0.074 ± 0.002	0.075 ± 0.002	0.078 ± 0.002
$PIR_1^{****)}$	0.070 ± 0.012	0.062 ± 0.010	0.051 ± 0.010
$PIR_2^{****)}$	0.077 ± 0.004	0.076 ± 0.005	0.082 ± 0.004
$PAT_3^{****)}$	0.073 ± 0.007	0.072 ± 0.005	0.081 ± 0.006
$PAT_4^{****)}$	0.085 ± 0.005	0.073 ± 0.007	0.080 ± 0.004
PAT_5	0.067 ± 0.007	0.074 ± 0.007	0.079 ± 0.007
PAT_6	0.071 ± 0.005	0.069 ± 0.003	0.066 ± 0.005
PAT_7	0.072 ± 0.003	0.067 ± 0.003	0.069 ± 0.003
PAT_8	0.070 ± 0.005	0.065 ± 0.005	0.070 ± 0.005
PIR_3	0.086 ± 0.003	0.070 ± 0.005	0.070 ± 0.005

Table 4.6 Continued.

Signal	S	κ_1	S_-
n1	0.143±0.003*)	0.115±0.003*)	0.127±0.004
n2	0.103±0.003*)	0.093±0.003*)	0.122±0.003
n3	0.117±0.010*)	0.100±0.008*)	0.118±0.010
n4	0.106±0.010*)	0.100±0.013*)	0.138±0.010
n5	0.091±0.011*)	0.086±0.007*)	0.120±0.011
n6	0.102±0.007*)	0.084±0.004*)	0.095±0.007
n7	0.116±0.005	0.085±0.005	0.083±0.005
n8	0.117±0.004	0.095±0.007	0.099±0.005
n9	0.110±0.010	0.091±0.005	0.095±0.010
n10	0.112±0.005	0.087±0.007	0.087±0.006
n11	0.122±0.012	0.088±0.007	0.079±0.012
n12	0.104±0.005	0.094±0.005	0.103±0.009
n13	0.124±0.007	0.084±0.007	0.077±0.008
n14	0.124±0.005	0.087±0.005	0.081±0.007

*) From Ref. [33] and mentioned in Fig. 2.8.
**) From Ref. [41].
***) From Ref. [40].
****) From Ref. [39].

In other words, the SES activities can be distinguished from "artificial" noises by considering that for the SES activities *both* S and S_- are smaller than S_u, which is *not* the case for "artificial" noises , i.e.,

$$S, S_- < S_u \text{ for SES activities} \tag{4.32}$$

This happens *in addition to* the fact that for the SES activities the variance κ_1 is $\kappa_1 \approx 0.070$, while for "artificial" noises we have $\kappa_1 \geq \kappa_u \approx 0.083$, see § 4.2.2.

4.9.2 Distinction of SES activities from "artificial" noises on the basis of the fluctuations of natural time under time reversal

In § 2.2.2, it was discussed that a measure of the long-range dependence emerges in natural time if we study the dependence of the fluctuations of the average value of natural time under time reversal

$$\Delta\chi_l^2 \equiv \mathscr{E}[(\langle\chi\rangle - \langle\hat{T}\chi\rangle)^2] = \mathscr{E}\left\{\left[\sum_{k=1}^{l}\frac{k}{l}(p_k - p_{l-k+1})\right]^2\right\}, \tag{4.33}$$

on the window length l that is used for the calculation. In particular, it was shown that Eq. (2.19) holds, i.e,

$$\Delta\chi_l (\equiv \sqrt{\Delta\chi_l^2}) \propto l^{\chi_H} \tag{4.34}$$

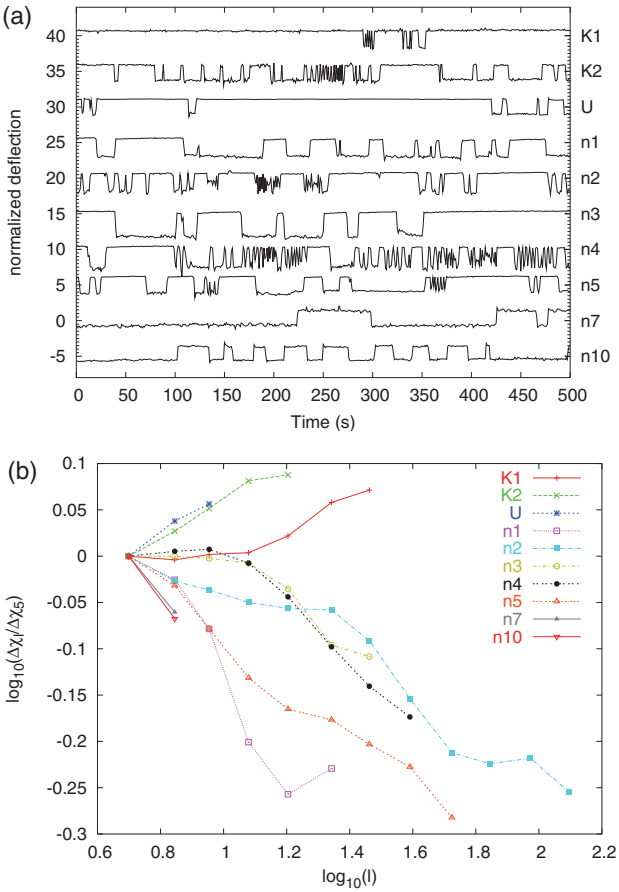

Fig. 4.23 The log-log plot of $\Delta\chi_l$ versus the scale l is depicted in (b) for three SES activities (K1, K2 and U) and seven "artificial" noises (n1-n5, n7 and n10) excerpts of which are shown in (a). The values of $\Delta\chi_l$ are divided by the corresponding values $\Delta\chi_5$ at the scale $l = 5$. Reprinted with permission from Ref. [39]. Copyright (2008), American Institute of Physics.

Hence, the scaling exponent χ_H can be determined from the slope of the $\log\Delta\chi_l$ versus $\log l$ plot. Recall also that in such a plot, we have the interconnection:

$$\chi_H \approx H - 1 \quad \text{for descending curves} \tag{4.35}$$

or

$$\chi_H = H \quad \text{for ascending curves} \tag{4.36}$$

We now show [39] that the aforementioned scale-dependence of the fluctuations of the natural time itself under time reversal provides a useful tool for the discrimination of SES activities from "artificial" noises. We apply this procedure to the time series of the durations of those signals analyzed in Ref. [43] that have enough number of pulses e.g. $\approx 10^2$, excerpts of which are depicted here in Fig. 4.23(a). The relevant results are shown in Fig. 4.23(b). An inspection of this figure interestingly indicates that *all* seven "artificial" noises correspond to *descending* $\Delta\chi_l$ curves versus the scale l, while the three SES activ-

ities to *ascending* curves (in a similar fashion as in Figs. 2.3(a) and 2.3(d), respectively) as expected from the fact that the latter exhibit [34] infinitely ranged temporal correlations (having H close to unity), while the former do not.

Hence, the method discussed here, which is based on the fluctuations of the average value of the natural time itself under time reversal, enables the identification of long-range correlations *even for datasets of small size* ($\approx 10^2$), thus allowing the distinction of SES activities from "artificial" noises.

4.10 Summary of the criteria in natural time for the distinction of SES activities from noise

By summarizing the previous Sections of this Chapter, the following three rules are put forward for the distinction between SES activities and "artificial" noises (AN).

First (note that each class of signals below is designated by the relevant subscript):

$$\kappa_{1,\mathrm{SES}} < \kappa_{1,ICFMC} (\approx \kappa_u) \leq \kappa_{1,\mathrm{AN}}, \tag{4.37}$$

where $\kappa_{1,ICFMC} \approx 0.080$ and $\kappa_u \approx 0.083$ and

$$\kappa_{1,\mathrm{SES}} \approx 0.070. \tag{4.38}$$

Second,

$$S_{\mathrm{SES}}, \;\; (S_-)_{\mathrm{SES}} < S_u \leq S_{\mathrm{AN}}, \tag{4.39}$$

where S and S_- stand for the entropy in natural time and that under time reversal, respectively; the value S_u is the one of the "uniform" distribution, i.e., $S_u \approx 0.0966$. The S values themselves are used for the distinction when they differ markedly from S_u. On the other hand, if the S values are found to be close to S_u, which holds for the minority of the SES activities and the AN, the distinction can be better made by using the complexity measure λ_s of the fluctuations δS of the entropy (see § 4.8.3).

Third, if H denotes the generalized Hurst exponent $h(2)$ in natural time,

$$H_{\mathrm{AN}} < H_{\mathrm{SES}}, \tag{4.40}$$

where H_{SES} is close to unity, i.e,

$$H_{\mathrm{SES}} \approx 1.0 \tag{4.41}$$

and $H_{\mathrm{AN}} \leq 0.86$.

The same holds for the DFA exponent in natural time, i.e.,

$$0.86 < \alpha_{SES} \approx 1.0 \tag{4.42}$$

and

$$\alpha_{AN} = 0.65 - 0.80. \tag{4.43}$$

A safe distinction between SES activities and AN should not be solely based on the above three rules but should be used *in conjunction with* the criteria explained in Section 1.2. The basic spirit behind these rules is that SES activities exhibit critical behavior while AN do not. Some types of AN, however, may be also associated with criticality (e.g., when a "man-made" system approaches failure) and hence could in principle be misinterpreted on the basis of the above inequalities.

4.11 Procedure to analyze a long-duration SES activity in natural time

When a short duration SES activity has an obvious dichotomous nature, the procedure to read it in natural time is straightforward, i.e., the one shown in Fig. 2.1(a) where we considered Q_k as being proportional to the duration of the k-th pulse. This is the case, for example, of the SES activity recorded at IOA on April 18, 1995, whose original time series is shown in Fig. 1.11(a) (and see its excerpt in Fig. 4.2(a)), while Fig. 4.6 depicts how this SES activity is read in natural time.

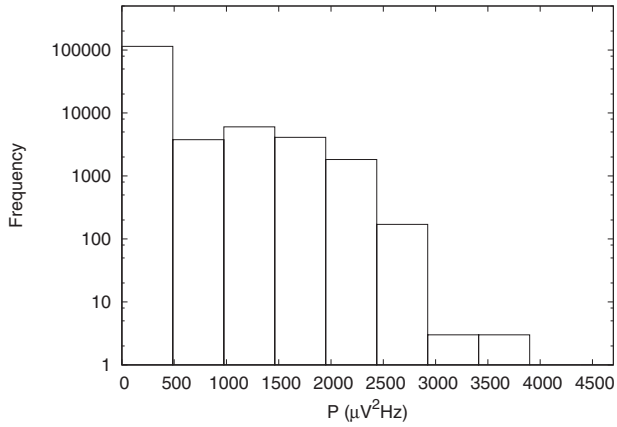

Fig. 4.24 Histogram of the "instantaneous power" P, i.e., the squared amplitude of the signal depicted in channel "e" of Fig. 1.16. Reprinted with permission from Ref. [35]. Copyright (2009), American Institute of Physics.

We now focus on a long-duration SES activity of a non-obvious dichotomous nature which is superimposed on a background that exhibits frequent small MT variations. Let us consider, for example, the SES activity that lasted from February 29 until March 2, 2008 (channel "a" of Fig. 1.16), for which the procedure to subtract the MT background variations has already been presented in § 1.4.3.1. This subtraction results in channel "e" of Fig. 1.16, which provides the time series that should be now analyzed in natural time: To obtain the time series (χ_k, Q_k), the individual pulses of the signal depicted in channel "e" of Fig. 1.16 have to be identified. A pulse starts, of course, when the amplitude exceeds a given threshold and ends when the amplitude falls below it. Moreover, since the signal is not obviously dichotomous, instead of finding the duration of each pulse, one should sum the "instantaneous power" during the pulse duration in order to find Q_k. To this end, we

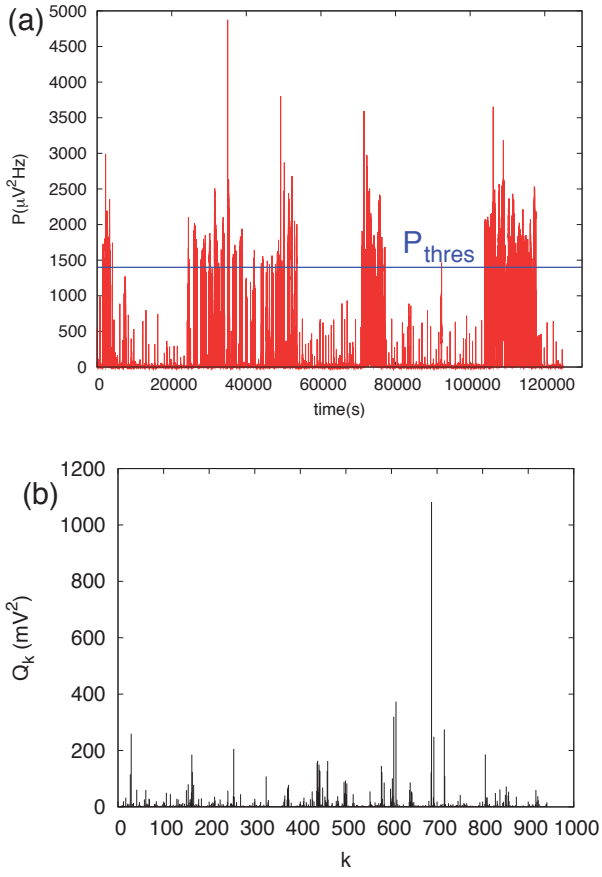

Fig. 4.25 (a) The "instantaneous power" P of the signal depicted in channel "e" of Fig. 1.16 (computed by squaring its amplitude). The solid line parallel to the x-axis marks an example of a threshold P_{thres} ($= 1400\ \mu V^2$ Hz) chosen. (b) The resulting representation of the signal depicted in channel "e" of Fig. 1.16 in natural time, when considering $P_{thres} = 1400\ \mu V^2$ Hz. Reprinted with permission from Ref. [35]. Copyright (2009), American Institute of Physics.

plot in Fig. 4.24 the histogram of the "instantaneous power" P of channel "e" of Fig. 1.16, computed by squaring its amplitude. An inspection of this figure reveals a bimodal feature which signifies the periods of inactivity ($P < 500\ \mu V^2$ Hz) and activity ($P > 500\ \mu V^2$ Hz) in channel "e" of Fig. 1.16. In order to find Q_k, we focus on the periods of activity and select the power threshold P_{thres} around the second peak of the histogram in Fig. 4.24. Let us consider, for example, the case of $P_{thres} = 1400\ \mu V^2$Hz. In Fig. 4.25(a), we depict the "instantaneous power" P of the signal in channel "e" of Fig. 1.16 versus time. Starting from the beginning of the signal, we compare P with P_{thres} and when P exceeds P_{thres} we start summing the P values until P falls below P_{thres} for the first time, $k = 1$. The resulting sum corresponds to Q_1. This procedure is repeated until P falls below P_{thres} for the second time, $k = 2$, and the new sum represents Q_2, etc. This leads to the natural time representation depicted in Fig. 4.25(b). The result depends, of course, on the proper selection of P_{thres}. The latter should be verified by checking whether a small change of P_{thres} around the second peak of the histogram leads to a natural time representation resulting in approximately the same values of the parameters κ_1, S and S_-. By randomly selecting

P_{thres} in the range 500 to 2,000 μV^2 Hz, we obtain that the number of pulses in channel "e" of Fig. 1.16 is $N = 1{,}100 \pm 500$ with $\kappa_1 = 0.070 \pm 0.007$, $S = 0.082 \pm 0.012$ and $S_- = 0.078 \pm 0.006$. When P_{thres} ranges between 1,000, and 1,500 μV^2 Hz, the corresponding values are $N = 1{,}200 \pm 200$ with $\kappa_1 = 0.068 \pm 0.003$, $S = 0.080 \pm 0.005$ and $S_- = 0.074 \pm 0.003$. Thus, we observe that irrespective of the P_{thres} value chosen, the parameters κ_1, S and S_- obey the conditions (4.38) and (4.39) for the classification of this signal as SES activity.

To summarize: natural time analysis allows the distinction between true SES activities and "artificial" (man-made) signals. This type of analysis, however, demands the knowledge of the energy released during each consecutive event. (Note that the determination of this energy is easier to conduct in the case of electric field variations, because the magnetic field variations appear in the form of "spikes" when using coil magnetometers which, as mentioned in § 1.4.4, act as dB/dt detectors.) *If* these electric field variations are of clear dichotomous nature, the energy release is proportional to the duration of each pulse. Otherwise, in the absence of an obvious dichotomous nature, an analysis of the "instantaneous power" similar to that presented above should be carried out to determine the parameters κ_1, S and S_- in natural time.

Acknowledgments We thank Professor P.N.R. Usherwood and Dr. I. Mellor for providing us with the experimental data of ion current through high-conductance locust potential channel.

References

1. Abramowitz, M., Stegun, I.: Handbook of Mathematical Functions. Dover, New York (1970)
2. Abry, P., Flandrin, P., Taqqu, M.S., Veitch, D.: Wavelets for the analysis, estimation and synthesis of scaling data. In: K. Park, W. Willinger (eds.) Self Similar Network Traffic Analysis and Performance Evaluation. Wiley, New York (2000)
3. Abry, P., Veitch, D., Flandrin, P.: Long-range dependence: Revisiting aggregation with wavelets. J. Time Ser. Anal. **19**, 253–266 (1998)
4. Audit, B., Bacry, E., Muzy, G., Arneodo, A.: Wavelet-based estimators of scaling behavior. IEEE Trans. Inf. Theory **48**, 2938-2954 (2002)
5. Bashan, A., Bartsch, R., Kantelhardt, J.W., Havlin, S.: Comparison of detrending methods for fluctuation analysis. Physica A **387**, 5080–5090 (2008)
6. Berezhkovskii, A.M., Weiss, G.H.: Detailed description of a two-state non-Markov system. Physica A **303**, 1-12 (2002)
7. Chen, Z., Ivanov, P.C., Hu, K., Stanley, H.E.: Effect of nonstationarities on detrended fluctuation analysis. Phys. Rev. E **65**, 041107 (2002)
8. Fuliński, A.: Active transport in biological membranes and stochastic resonances. Phys. Rev. Lett. **79**, 4926–4929 (1997)
9. Fuliński, A., Grzywna, Z., Mellor, I., Siwy, Z., Usherwood, P.N.R.: Non-Markovian character of ionic current fluctuations in membrane channels. Phys. Rev. E **58**, 919-924 (1998)
10. Gorczynska, E., Huddie, P., Miller, B., Mellor, I., Vais, H., Ramsey, R., Usherwood, P.: Potassium channels of adult locust (*Schistocerca gregaria*) muscle. Pflügers Archiv European Journal of Physiology **432**, 597–606 (1996)

11. Haar, A.: Zur theorie der orthogonalen funktionensysteme. (erste mitteilung). Mathematische Annalen **69**, 331–372 (1909)
12. Hu, K., Ivanov, P.C., Chen, Z., Carpena, P., Stanley, H.E.: Effect of trends on detrended fluctuation analysis. Phys. Rev. E **64**, 011114 (2001)
13. Hurst, H.E.: Long-term storage capacity of reservoirs. Trans. Am. Soc. Civ. Eng. **116**, 770–808 (1951)
14. Ivanov, P.C., Amaral, L.A.N., Goldberger, A.L., Havlin, S., Rosenblum, M.G., Stanley, H.E., Struzik, Z.R.: From 1/f noise to multifractal cascades in heartbeat dynamics. CHAOS **11**, 641–652 (2001)
15. Kantelhardt, J., Zschiegner, S.A., Koscienly-Bunde, E., Bunde, A., Havlin, S., Stanley, H.E.: Multifractal detrended fluctuation analysis of nonstationary time series. Physica A **316**, 87–114 (2002)
16. Kantelhardt, J.W., Koscielny-Bunde, E., Rego, H.H.A., Havlin, S., Bunde, A.: Detecting long-range correlations with detrended fluctuation analysis. Physica A **295**, 441–454 (2001)
17. Legendre, P.: K-means: Least squares partitioning method. Computer code K-Means available from http://www.bio.umontreal.ca/casgrain/en/labo/k-means.html (2001)
18. Legendre, P., Legendre, L.: Numerical Ecology. Elsevier, Amsterdam (1998)
19. Louis, A.K., Maass, P., Rieder, A.: Wavelets: Theory and Applications. Wiley, New York (1997)
20. Mandelbrot, B.B.: Gaussian Self-Affinity and Fractals. Springer-Verlag, New York (2002)
21. Mercik, S., Weron, K.: Stochastic origins of the long-range correlations of ionic current fluctuations in membrane channels. Phys. Rev. E **63**, 051910 (2001)
22. Muzy, J.F., Bacry, E., Arneodo, A.: The multifractal formalism revisited with wavelets. Int. J. Bifurcation CHAOS **4**, 245–302 (1994)
23. Siwy, Z., Fuliński, A.: Origin of $1/f^{\alpha}$ in membrane channel currents. Phys. Rev. Lett. **89**, 158101 (2002)
24. Siwy, Z., Mercik, S., Weron, K., Ausloos, M.: Application of dwell-time series in studies of long-range correlation in single channel ion transport: analysis of ion current through a big conductance locust potassium channel. Physica A **297**, 79–96 (2001)
25. Talkner, P., Weber, R.O.: Power spectrum and detrended fluctuation analysis: Application to daily temperatures. Phys. Rev. E **62**, 150–160 (2000)
26. Taqqu, M.S., Teverovsky, V., Willinger, W.: Estimators for long-range dependence: An empirical study. Fractals **3**, 785–798 (1995)
27. Varotsos, P.: The Physics of Seismic Electric Signals. TERRAPUB, Tokyo (2005)
28. Varotsos, P.A., Sarlis, N.V., Skordas, E.S.: See (the freely available) EPAPS Document No. E-PLEEE8-68-116309 originally from P.A. Varotsos, N.V. Sarlis and E.S. Skordas, *Phys. Rev. E* **68**, 031106 (2003). For more information on EPAPS, see http://www.aip.org/pubservs/epaps.html.
29. Varotsos, P.A., Sarlis, N.V., Skordas, E.S.: See (the freely available) EPAPS Document No. E-PLEEE8-67-110302 originally from P.A. Varotsos, N.V. Sarlis and E.S. Skordas, *Phys. Rev. E* **67**, 021109 (2003). For more information on EPAPS, see http://www.aip.org/pubservs/epaps.html.
30. Varotsos, P.A., Sarlis, N.V., Skordas, E.S.: Seismic Electric Signals and $1/f$ "noise" in natural time. arXiv:0711.3766v3 [cond-mat.stat-mech] (1 February 2008)
31. Varotsos, P.A., Sarlis, N.V., Skordas, E.S.: Spatio-temporal complexity aspects on the interrelation between Seismic Electric Signals and Seismicity. Practica of Athens Academy **76**, 294–321 (2001)
32. Varotsos, P.A., Sarlis, N.V., Skordas, E.S.: Long-range correlations in the electric signals that precede rupture. Phys. Rev. E **66**, 011902 (2002)
33. Varotsos, P.A., Sarlis, N.V., Skordas, E.S.: Attempt to distinguish electric signals of a dichotomous nature. Phys. Rev. E **68**, 031106 (2003)
34. Varotsos, P.A., Sarlis, N.V., Skordas, E.S.: Long-range correlations in the electric signals that precede rupture: Further investigations. Phys. Rev. E **67**, 021109 (2003)
35. Varotsos, P.A., Sarlis, N.V., Skordas, E.S.: Detrended fluctuation analysis of the magnetic and electric field variations that precede rupture. CHAOS **19**, 023114 (2009)
36. Varotsos, P.A., Sarlis, N.V., Skordas, E.S., Lazaridou, M.S.: See (the freely available) EPAPS Document No. E-PLEEE8-71-134501 originally from P.A. Varotsos, N.V. Sarlis, E.S. Skordas and M.S. Lazaridou *Phys. Rev. E* **71**, 011110 (2005). For more information on EPAPS, see http://www.aip.org/pubservs/epaps.html.
37. Varotsos, P.A., Sarlis, N.V., Skordas, E.S., Lazaridou, M.S.: Entropy in natural time domain. Phys. Rev. E **70**, 011106 (2004)

38. Varotsos, P.A., Sarlis, N.V., Skordas, E.S., Lazaridou, M.S.: Natural entropy fluctuations discriminate similar-looking electric signals emitted from systems of different dynamics. Phys. Rev. E **71**, 011110 (2005)
39. Varotsos, P.A., Sarlis, N.V., Skordas, E.S., Lazaridou, M.S.: Fluctuations, under time reversal, of the natural time and the entropy distinguish similar looking electric signals of different dynamics. J. Appl. Phys. **103**, 014906 (2008)
40. Varotsos, P.A., Sarlis, N.V., Skordas, E.S., Tanaka, H.K., Lazaridou, M.S.: Attempt to distinguish long-range temporal correlations from the statistics of the increments by natural time analysis. Phys. Rev. E **74**, 021123 (2006)
41. Varotsos, P.A., Sarlis, N.V., Skordas, E.S., Tanaka, H.K., Lazaridou, M.S.: Entropy of seismic electric signals: Analysis in the natural time under time reversal. Phys. Rev. E **73**, 031114 (2006)
42. Varotsos, P.A., Sarlis, N.V., Tanaka, H.K., Skordas, E.S.: See (the freely available) EPAPS Document No. E-PLEEE8-71-081503 originally from P.A. Varotsos, N.V. Sarlis, H.K. Tanaka and E.S. Skordas, *Phys. Rev. E* **71**, 032102 (2005). For more information on EPAPS, see http://www.aip.org/pubservs/epaps.html.
43. Varotsos, P.A., Sarlis, N.V., Tanaka, H.K., Skordas, E.S.: Some properties of the entropy in the natural time. Phys. Rev. E **71**, 032102 (2005)
44. Veitch, D., Abry, P.: A wavelet-based joint estimator of the parameters of long-range dependence. IEEE Trans. Inf. Theory **45**, 878–897 (1999)
45. Veitch, D., Abry, P., Chainais, P.: Wavelet estimation tools. Computer codes `Wavelet Estimation Tools` available from http://www.cubinlab.ee.unimelb.edu.au/∼darryl/ (2002)
46. Weber, R.O., Talkner, P.: Spectra and correlations of climate data from days to decades. J. Geophys. Res. **106(D17)**, 20,131–20,144 (2001)
47. Weiss, G.H.: Some applications of persistent random walks and the telegrapher's equation. Physica A **311**, 381–410 (2002)
48. Weron, A., Burnecki, K., Mercik, S., Weron, K.: Complete description of all self-similar models driven by Lévy stable noise. Phys. Rev. E **71**, 016113 (2005)
49. Willinger, W., Taqqu, M., Sherman, R., Wilson, D.: Self-similarity through high variability: Statistical analysis of ethernet LAN traffic at the source level. IEEE/ACM Trans. on Networking **5**, 71–86 (1997)